SANDIA REPORT
SAND2021-5811
Printed May 2021

Sandia National Laboratories

Validation and Comparison of HyRAM Physics Models

Brian D. Ehrhart, Ethan S. Hecht, Jamal A. Mohmand

Prepared by
Sandia National Laboratories
Albuquerque, New Mexico 87185
Livermore, California 94550

Issued by Sandia National Laboratories, operated for the United States Department of Energy by National Technology & Engineering Solutions of Sandia, LLC.

Available to DOE and DOE contractors from

U.S. Department of Energy
Office of Scientific and Technical Information
P.O. Box 62
Oak Ridge, TN 37831

Telephone: (865) 576-8401
Facsimile: (865) 576-5728
E-Mail: reports@osti.gov
Online ordering: http://www.osti.gov/scitech

Available to the public from

U.S. Department of Commerce
National Technical Information Service
5301 Shawnee Road
Alexandria, VA 22312

Telephone: (800) 553-6847
Facsimile: (703) 605-6900
E-Mail: orders@ntis.gov
Online order: https://classic.ntis.gov/help/order-methods

ABSTRACT

The Hydrogen Risk Assessment Models (HyRAM) software version 3 uses a real gas equation of state rather than the Abel-Noble equation of state that is used in 2.0 and previous versions. This change enables the use of HyRAM 3 for cryogenic hydrogen flows, whereas the Abel-Noble equation of state is not accurate at low temperatures. HyRAM 3.1 results were compared to experimental data from the literature in order to demonstrate the accuracy of the physics models. HyRAM 3.1 results were also compared to HyRAM 2.0 for high-pressure, non-cryogenic flows to highlight the differences in predictions between the two major versions of HyRAM. Validation data sets are from multiple groups and span the range of HyRAM physics models, including tank blowdown, unignited dispersion jet plume, ignited jet flame, and accumulation and overpressure inside an enclosure. Both versions 2.0 and 3.1 of HyRAM are accurate for predictions of blowdowns, diffusion jets, and diffusion flames of hydrogen at pressures up to 900 bar, and HyRAM 3.1 also shows good agreement with cryogenic hydrogen data. Overall, HyRAM 3.1 improves on the accuracy of the physical models relative to HyRAM 2.0. In most cases, this reduces the conservatism in risk calculations using HyRAM.

ACKNOWLEDGMENT

This work was supported by the U.S. Department of Energy (DOE), Office of Energy Efficiency and Renewable Energy (EERE), Hydrogen and Fuel Cell Technologies Office (HFTO). The authors wish to thank Myra Blaylock and Chris LaFleur from Sandia National Laboratories for peer reviewing this report.

CONTENTS

1. Introduction 13
   1.1. Background and Motivation 13
   1.2. Overview of Changes 14
      1.2.1. Equation of State Calculations 14
      1.2.2. Other Model Updates 14
   1.3. Comparison Analysis 15

2. Methodology 17

3. Results and Discussion 19
   3.1. Blowdowns 19
   3.2. Unignited Jet Plumes 24
   3.3. Ignited Jet Fires 33
   3.4. Accumulation and Overpressure in Enclosures 40
   3.5. Cryogenic Releases 46
      3.5.1. Blowdowns 46
      3.5.2. Unignited Jet Plumes 52
      3.5.3. Ignited Jet Fires 60

4. Conclusions 63

References 65

Appendix A. Validation Data Input Parameters 69
   A.1. Blowdown Input Parameters 69
   A.2. Unignited Jets/Gas Plumes Input Parameters 70
   A.3. Ignited Jet Fires Input Parameters 74
   A.4. Indoor Accumulation and Overpressure Input Parameters 79
   A.5. Cryogenic Hydrogen Input Parameters 88
      A.5.1. Blowdown 88
      A.5.2. Unignited Jet Plumes 89
      A.5.3. Ignited Jet Fires 91

LIST OF FIGURES

Figure 3-1. Flow rate data during blowdown from Ekoto et al. [19] compared to HyRAM models 20
Figure 3-2. Pressure data during blowdown from Schefer et al. [20] compared to HyRAM models 21
Figure 3-3. Tank pressures and temperatures during blowdown from Proust et al. [21] compared to HyRAM models 22

Figure 3-4. Mass flow rate data for a blowdown from Schefer et al. [22] compared to HyRAM predictions 23
Figure 3-5. Centerline mass fractions from data compiled by Molkov [23]. In the legends, T denotes temperature (K), d denotes diameter (mm), and P denotes pressure (MPa). Lines are results from HyRAM, with the same colors as the conditions in the legends. The dashed lines are from HyRAM 2.0 while the solid lines are from HyRAM 3.1. 26
Figure 3-6. Radial profiles of mass fraction at several downstream locations reported by Houf and Schefer [6] (symbols) compared to HyRAM 2.0 and 3.1 (lines) 27
Figure 3-7. Inverse centerline mole fraction as a function of downstream distance as reported by Houf and Schefer [6] (symbols) and predicted by HyRAM (lines) . . . 28
Figure 3-8. Inverse centerline mass fraction and half-width as a function of normalized downstream distance from Ruggles and Ekoto [24] compared to HyRAM 2.0 (dashed lines) and HyRAM 3.1 (solid lines) 29
Figure 3-9. Data for 100–400 bar jets, as reported by Han et al. [25] compared to HyRAM. 30
Figure 3-10. Inverse centerline mole fraction as reported by Han et al. [25] compared to HyRAM 31
Figure 3-11. Heat flux during a blowdown as reported by Schefer et al. [22] (symbols) and predicted by HyRAM (lines) 34
Figure 3-12. Data from Houf and Schefer [9] compared to HyRAM 35
Figure 3-13. HyRAM comparisons to data from Imamura et al. [32] 36
Figure 3-14. Radiative heat flux values for different mass flowrates from Mogi et al. [33] compared to HyRAM, in which d is the diameter of the orifice and L is the distance between the detector and flame axis 37
Figure 3-15. HyRAM simulations compared to data from from Proust et al. [21] during a 900 bar blowdown 38
Figure 3-16. Hydrogen mole fraction measurements from different sensors at the ceiling over multiple experiments with and without ventilation from Ekoto et al. [19] compared to HyRAM predictions 41
Figure 3-17. Overpressure values from Ekoto et al. [19] (thin, dashed lines) for igniting hydrogen mixtures 3 seconds after the start of the release (time of 0 is at the ignition time). Labels with respect to the colors relate to the ventilation, and HyRAM lines (thick) are the overpressure predictions for ignition after 3 seconds under the conditions described. 42
Figure 3-18. Hydrogen concentration measurements along the ceiling from Giannissi et al. [34] compared with HyRAM predictions 43
Figure 3-19. Hydrogen concentrations at different heights over time for tests with different hydrogen flowrates and garage open space from Merilo et al. [35] compared to HyRAM predictions. The upper two and lower left frames have only natural ventilation, while the bottom-right frame has 0.1 m^3/s mechanical ventilation. 44
Figure 3-20. Maximum hydrogen concentration values for different release flowrates and orifice sizes in enclosures, with data from Bernard-Michel and Houssin-Agbomson [36] compared to HyRAM 45

Figure 3-21. Pressure during discharge for vessel (blue) and nozzle (orange) for varied pressures, temperatures, and nozzle diameters from Friedrich et al. [39] (solid lines) compared to HyRAM 3.1 (dashed lines) 47
Figure 3-22. Temperature during discharge for vessel top (blue), vessel center (orange), vessel bottom (green), and nozzle (red) as measured by sheathed (thick line) and unsheathed (thin line) thermocouples for varied pressures, temperatures, and nozzle diameters from Friedrich et al. [39] (solid lines) compared to HyRAM 3.1 (dashed lines) 49
Figure 3-23. Tank mass during discharge from Friedrich et al. [39] (solid lines) compared to HyRAM 3.1 (dashed lines) 50
Figure 3-24. Inverse centerline mole fraction as a function of normalized downstream distance for four release scenarios, including two cryogenic (80 K) releases, using data (open circles) from Xiao et al. [37] compared to HyRAM 3.1 (solid lines) 52
Figure 3-25. Inverse centerline mole fraction as a function of normalized downstream distance from Friedrich et al. [38] (circles) compared to HyRAM 3.1 (lines) 53
Figure 3-26. Comparison of mole fraction calculated by HyRAM 3.1 (thin, solid lines) to cryogenic hydrogen dispersion data reported by Hecht and Panda [13] (shading and thick, dashed lines) as well as some previously unreported data 54
Figure 3-27. Comparison of temperatures calculated by HyRAM 3.1 (thin, solid lines) to cryogenic hydrogen dispersion data reported by Hecht and Panda [13] (shading and thick, dashed lines) as well as some previously unreported data 55
Figure 3-28. Correlation of data to HyRAM for all diameters, pressures, temperatures shown in Figures 3-26 and 3-27 (each point for counting purposes is a 0.5 mm $\times$ 0.5 mm pixel) 56
Figure 3-29. Molar concentrations during discharge for locations of r = 0 cm, z = 150 cm (blue); r = 0 cm, z = 100 cm (orange); r = 0 cm, z = 50 cm (green - thick and thin lines, with the thin line having a different cut on the extraction probe); and r = 10 cm, z = 100 cm (red) from Friedrich et al. [39] (solid lines) compared to HyRAM 3.1 (dashed lines) 57
Figure 3-30. Temperatures outside the vessel during discharge for locations of r = 2 cm, z = 20 cm (blue); r = 0 cm, z = 25 cm (orange); r = 5 cm, z = 50 cm (green); r = 0 cm, z = 75 cm (red); and r = 0 cm, z = 175 cm (purple) from Friedrich et al. [39] (solid lines) compared to HyRAM 3.1 (dashed lines) 59
Figure 3-31. Comparison of flame length calculated by HyRAM 3.1 to those measured by Panda and Hecht [12] 60
Figure 3-32. Comparison of heat flux (Q) calculated by HyRAM 3.1 to those measured by Panda and Hecht [12] 61

LIST OF TABLES

Table 3-1. Blowdown Validation Data Sources 19
Table 3-2. Unignited Jet Validation Data Sources 24
Table 3-3. Flame Validation Data Sources 33

Table 3-4. Flame Length and Heat Flux Results from Ekoto et al. [10] compared to HyRAM 33
Table 3-5. Overpressure/Accumulation Validation Data Sources 40
Table 3-6. Cryogenic Blowdown Validation Data Sources 46
Table 3-7. Cryogenic Unignited Jet Plumes Validation Data Sources 52
Table 3-8. Cryogenic Ignited Jet Plumes Validation Data Sources 60
Table A-1. Ekoto et al. [19] Figure 3 Input Parameters 69
Table A-2. Schefer et al. [20] Figure 4 Input Parameters 69
Table A-3. Proust et al. [21] Figure 4 Input Parameters 69
Table A-4. Schefer et al. [22] Figure 3b Input Parameters 69
Table A-5. Molkov [23] Table 5-3 Input Parameters 70
Table A-6. Houf and Schefer [6] Figure 5 Input Parameters 70
Table A-7. Houf and Schefer [6] Figure 8 Input Parameters 71
Table A-8. Houf and Schefer [6] Figure 9 Input Parameters 71
Table A-9. Ruggles and Ekoto [24] Figure 7 Input Parameters 71
Table A-10. Han et al. [25] Figure 3 Input Parameters 72
Table A-11. Han et al. [25] Figure 6 Input Parameters 72
Table A-12. Han et al. [25] Figure 7 Input Parameters 72
Table A-13. Han et al. [25] Figure 8 Input Parameters 73
Table A-14. Ekoto et al. [10] Table 2 Input Parameters 74
Table A-15. Schefer et al. [22] Figure 8 Input Parameters 75
Table A-16. Houf and Schefer [9] Figure 5 Input Parameters 75
Table A-17. Houf and Schefer [9] Figure 6 Input Parameters 76
Table A-18. Imamura et al. [32] Table 2 Input Parameters 77
Table A-19. Imamura et al. [32] Table 2 Input Parameters 77
Table A-20. Mogi et al. [33] Figure 9 Input Parameters 78
Table A-21. Proust et al. [21] Figure 8 Input Parameters 78
Table A-22. Proust et al. [21] Figure 10 Input Parameters 78
Table A-23. Ekoto et al. [19] Figure 9 Input Parameters 79
Table A-24. Ekoto et al. [19] Figure 9 Sensor Locations 80
Table A-25. Ekoto et al. [19] Figure 14 Input Parameters 81
Table A-26. Giannissi et al. [34] Figure 7 Input Parameters 82
Table A-27. Merilo et al. [35] Figure 2 Overall Input Parameters 83
Table A-28. Merilo et al. [35] Figure 2 Sub-Figure Specific Input Parameters 84
Table A-29. Merilo et al. [35] Figure 6a Input Parameters 85
Table A-30. Bernard-Michel and Houssin-Agbomson [36] Figure 7 Input Parameters 86
Table A-31. Bernard-Michel and Houssin-Agbomson [36] Figure 9 Input Parameters 87
Table A-32. Friedrich et al. [39] Dataset Input Parameters 88
Table A-33. Xiao et al. [37] Figure 3 Input Parameters 89
Table A-34. Friedrich et al. [38] Figure 5 Input Parameters 89
Table A-35. Hecht and Panda [13] Figure 10 Input Parameters 90
Table A-36. Panda and Hecht [12] Table 3 Input Parameters 91

EXECUTIVE SUMMARY

The Hydrogen Risk Assessment Models (HyRAM) software version 3 contains some significant changes over version 2.0 and earlier. Some of the most significant model changes enable HyRAM 3 to be used for cryogenic hydrogen releases, whereas the Abel-Noble equation of state used previously is not accurate at low temperatures. In this report, HyRAM 3.1 results were compared to experimental data from the literature in order to demonstrate the accuracy of the physics models. HyRAM 3.1 results were also compared to HyRAM 2.0 for high-pressure, non-cryogenic flows to compare the predictions between these two major versions of HyRAM. This includes comparisons of the original validation data to both HyRAM 2.0 and 3.1, as well as multiple additional experiments identified in the literature. Validation data sets are from multiple groups and span the range of HyRAM physics models, including tank blowdown, unignited dispersion jet plume, ignited jet flame, and accumulation and overpressure inside an enclosure.

The blowdown (emptying) of high-pressure, room-temperature tanks predicted by HyRAM 3.1 and 2.0 are compared to four literature sources that contain data for hydrogen tanks with initial pressures of 13.45 MPa, 15.5 MPa, 43.1 MPa, and 90 MPa. Values predicted by HyRAM 2.0 and 3.1 were nearly equivalent for pressure losses, flow rates, and times to empty for blowdowns. The predicted pressure losses, flow rates, and times to empty are also similar to experimental results. The tank temperature was also monitored in one experiment and in this case, both versions of HyRAM predict much lower tank temperatures than the experimental measurements. This is likely due to gas mixing within the tank and heat flow through the tank walls, which are not accounted for in either version of HyRAM. Gas temperatures inside a tank during a blowdown are generally not used in risk or hazard assessments, so this is not expected to significantly affect typical use-cases.

Mean concentrations (mole and mass fractions) during the dispersion of hydrogen are compared for a range of release scenarios. HyRAM 2.0 tends to predict mean centerline mole fractions that are greater than the literature data while HyRAM 3.1 generally provides better agreement along the centerline. This means that HyRAM 3.1 predicts a faster centerline concentration decay than HyRAM 2.0 in most scenarios, due to increased momentum driven entrainment in HyRAM 3.1 over HyRAM 2.0. Increased momentum driven entrainment and a faster centerline concentration decay reduces the dilution length (distance to a given concentration). Dilution length is generally used to specify distances in risk analyses, meaning that while HyRAM 3.1 is generally more accurate, it is less conservative than HyRAM 2.0 in this context. Neither version 2.0 nor 3.1 of HyRAM is particularly accurate at predicting the width of the Gaussian dispersion profile. Improved tuning of empirical parameter values within the HyRAM model may improve this agreement, but this needs to be explored further.

Flame lengths and heat fluxes for ignited high-pressure hydrogen diffusion flames are predicted and compared to a variety of literature data. Updates to HyRAM 3.1 from 2.0 do not significantly affect prediction of flame length or heat flux, with HyRAM 3.1 producing minimally more conservative values (a longer flame length and higher heat flux). Overall, both versions of HyRAM accurately predict both flame length and heat flux, for hydrogen diffusion flames up to 900 bar.

Accumulation within an enclosure and the overpressure that would result if the accumulated hydrogen were to ignite are compared to several literature sources. HyRAM 3.1 predicts similar or higher concentrations within an enclosure than HyRAM 2.0. In one case, HyRAM 2.0 predicted a lower peak overpressure than was measured experimentally for ignition of an accumulated mixture within an enclosure without ventilation, while HyRAM 3.1 predicted higher peak overpressures than were measured experimentally for all ventilation conditions. In another case, concentration values measured along the ceiling were higher than those predicted by both versions of HyRAM, likely due to local higher concentrations from impingement of the release-plume. Both versions of HyRAM 2.0 and 3.1 predict concentrations and overpressures that are similar to literature data, but there is a fairly wide variability in accuracy, depending on the exact experimental setup. This wide variability in prediction accuracy indicates that this accumulation and overpressure model should be used with caution. Careful consideration should be given to determining if the simplified model is appropriate for a given release scenario.

Finally, HyRAM 3.1 is compared to literature data for cryogenic releases of hydrogen. Only HyRAM 3.1 is compared to cryogenic releases due to the inapplicability of HyRAM 2.0 at the low temperatures. Similar to the room-temperature blowdown simulations, HyRAM 3.1 fairly accurately predicts the pressure decay as a tank is emptied, but predicts temperatures in the tank that are much lower than the measured experimental data. HyRAM 3.1 also predicts significant differences in the pressure and temperature in the orifice vs. the tank, while the pressure and temperature measured at the orifice and tank in one set of experiments were similar. HyRAM 3.1 predicts centerline concentration decay and even two-dimensional near-field concentration fields of unignited jets accurately. HyRAM 3.1 tends to slightly overpredict concentration at most points in the two-dimensional fields, while temperature measurements were both higher and lower than those predicted. In the two-dimensional experiments, the temperature measurements had more uncertainty than the concentration measurements. Similar to the warm releases, HyRAM 3.1 also predicts slightly longer visible flame lengths and heat fluxes than were measured experimentally.

Overall, HyRAM 3.1 improves on the accuracy of the physical models relative to HyRAM 2.0. This improvement tends to reduce the conservatism in hazard/risk calculations using HyRAM. Both versions 2.0 and 3.1 of HyRAM are accurate for predictions of blowdowns, diffusion jets, and diffusion flames of hydrogen at pressures up to 900 bar, and HyRAM 3.1 also shows good agreement with cryogenic hydrogen data. Improvements could be made to the two-dimensional (width) of the dispersion predictions as well as the indoor accumulation and overpressure models. As additional data for cryogenic hydrogen behavior becomes available, additional comparisons and model improvements should be made.

ACRONYMS AND DEFINITIONS

DOE Department of Energy

EERE Office of Energy Efficiency and Renewable Energy

HFTO Hydrogen and Fuel Cell Technologies Office

HyRAM Hydrogen Risk Assessment Models

LFL lower flammability limit

NIST National Institute of Standards and Technology

PreSLHy Prenormative Research for Safe Use of Liquid Hydrogen

REFPROP Reference Fluid Thermodynamic and Transport Properties Database

This page intentionally left blank.

1. INTRODUCTION

1.1. Background and Motivation

The Hydrogen Risk Assessment Models (HyRAM) software and its documentation was originally published in 2015 (version 1.0) [1] and then updated in 2017 (version 1.1) [2], 2019 (version 2.0) [3], 2020 (version 3.0) [4], and 2021 (version 3.1) [5]. It contains both quantitative risk assessment and physics models for hydrogen releases. The physics models can be used to simulate the behavior of a gaseous (and in versions ≥ 3.0, saturated vapor or saturated liquid) hydrogen release for both unignited jet plumes, ignited jet flames, and accumulation in an enclosure. The unignited and ignited jets are based on models developed, validated, and published at Sandia National Laboratories, although many of the underlying models were developed elsewhere. Specifically, the unignited jet plume follows a one-dimensional model described by Houf and Schefer [6] (version ≤ 2.0) and Houf and Winters [7, 8]. For the heat flux from a jet flame, an engineering correlation developed by Houf and Schefer [9] is used for straight flames. A similar model to the jet/plume is used to simulate a flame as described by Ekoto et al. [10]. An updated approximation for heat flux from curved flames uses a weighted multi-source model, similar to that described by Hankinson and Lowesmith [11], to calculate the total heat flux at each point along the flame length.

Before version 3.0, HyRAM used the Abel-Noble equation of state as a simple and accurate relationship between pressure, temperature, and volume for gaseous hydrogen that is more accurate than the ideal gas law over a wider range of conditions. When compared to the NIST Standard Reference Database 23 (REFPROP), the Abel-Noble equation of state has been shown to be accurate for hydrogen at pressures less than 200 MPa and temperatures greater than 150 K [1]. This temperature limitation on accuracy meant that the Abel-Noble equation of state should not be used for cryogenic releases of liquid hydrogen (which are around 20–30 K). An experimental effort was undertaken to quantify the behavior of cryogenic releases of hydrogen, and the resulting data was then compared to a modified version of the models in HyRAM [12–14]. The major difference in these models was the use of a real gas equation of state to relate pressure, temperature, and volume. This equation of state is accurate for high pressures and low temperatures, and good agreement was achieved between experimental data and the simulation.

When the updated results from HyRAM models with the real gas equation of state (version ≥ 3.0) were compared to the previous HyRAM versions (≤ 2.0), the results differed even for high-pressure, ambient-temperature hydrogen releases. Therefore, this report reexamines the validation data used for HyRAM, comparing both versions 3 and 2 to that data. The original validation data consisted of a limited number of release scenarios that were compared to the HyRAM predictions. Thus, additional validation data were needed to compare to both versions of the HyRAM models. Cryogenic hydrogen release data were also needed for the validation of versions ≥ 3.0; given the temperature limitation of prior versions of HyRAM, this cryogenic release data is only applicable for version 3.0 and above.

1.2. Overview of Changes

1.2.1. Equation of State Calculations

The Abel-Noble equation of state used in HyRAM versions ≤ 2.0 is similar to the ideal gas equation of state, but includes a co-volume constant to account for intermolecular interactions at high pressure. With this form of the equation of state, analytic expressions can be found for the temperature or density for isentropic flow through an orifice, or the speed of sound, as documented in previous HyRAM Technical Reference Manuals [1, 2]. While this equation of state is accurate at high pressures (up to 200 MPa), significant deviations occur at low temperatures (less than 150 K).

The real gas equation of state for hydrogen used by HyRAM versions ≥ 3.0 is based on the work of Leachman et al. [15], which is accurate for hydrogen at pressures below 2000 MPa and temperatures between 14 and 1000 K. This equation of state is explicit in the Helmholtz free energy, with an ideal gas contribution and a residual contribution. Derived properties, including the density, enthalpy, entropy, and speed of sound, are calculated from derivatives of the Helmholtz free energy. The calculations are accurate for both gas- and liquid-phase hydrogen. The property calculations are made through the CoolProp interface [16] in Python. These properties are used to calculate aspects of the release such as isentropic flow through an orifice, expansion of a notional nozzle, a tank blowdown, etc., as described in the technical reference manual [4].

1.2.2. Other Model Updates

HyRAM versions ≥ 3.0 can handle cryogenic hydrogen, which is well below the freezing point of oxygen and nitrogen from the air. As noted by Houf and Winters [8], there are challenges calculating properties in regions of the flow where oxygen and nitrogen from the entrained air would condense due to the extremely low temperatures. Therefore, HyRAM 3.0 introduced an additional "zone of initial entrainment and heating," used only when the temperature is below the freezing point of oxygen and nitrogen, to heat the mixture in this region to a temperature that the equation of state can handle. It should be noted that this zone is not used for room temperature releases, and will therefore not be responsible for any differences between HyRAM ≥ 3.0 and HyRAM ≤ 2.0 at room temperature. This is because HyRAM ≤ 2.0 is only valid for temperatures above 150 K, well above the freezing point of oxygen and nitrogen.

Previously, when an expanded plug node (after the notional nozzle model) developed into the Gaussian profiles of velocity and density (or mixture fraction, for the flame model), the temperature was assumed to be ambient. Because HyRAM versions ≥ 3.0 can now handle cryogenic hydrogen, the centerline temperature is calculated and can be below ambient temperature. The HyRAM ≥ 3.0 calculations for the zone of flow establishment are more similar to HyRAM versions 1.0 and 1.1, while HyRAM 2.0 used correlations described by Li et al. [17].

In the Jet/Plume model of HyRAM ≥ 3.0, momentum driven entrainment is based on the conditions at the expanded plug node (after the notional nozzle model and zone of initial entrainment and heating, if needed), while for HyRAM ≤ 2.0, the entrainment was calculated based on the conditions at the orifice. The entrainment model in HyRAM ≥ 3.0 results in slightly more entrainment than the previous version. In addition, HyRAM ≥ 3.0 includes an equation conserving energy as the Gaussian shaped velocity and density profiles are transported downstream. This additional conservation equation enables the temperature to change in the fully developed flow section.

1.3. Comparison Analysis

This report details an expanded validation comparison effort undertaken to compare the effects of model updates on the HyRAM physics models. This includes comparisons of the original validation data to both HyRAM 2 and 3, as well as multiple additional experiments identified in the literature. Validation data sets are from multiple groups and span the range of HyRAM physics models, including tank blowdown, unignited dispersion jet plume, ignited jet flame, and accumulation and overpressure inside an enclosure. The literature sources themselves are described, along with the specific model inputs used in order to match the experimental conditions. Then results of the two versions of the HyRAM physics models are compared against these experimental data to see the level of agreement.

This page intentionally left blank.

2. METHODOLOGY

Literature sources of experimental data for validation comparison were identified for each of the different physics models within HyRAM. These sources include the original validation data listed in the HyRAM technical reference manuals [1, 2, 4] and the sources cited therein. A literature search was also performed to identify additional sources, including those that were not published when the original model validations were performed (prior to HyRAM version 1.0). Once the literature data sources for each different physics model were identified, the data from the graphs needed to be digitized. An online tool, WebPlotDigitizer, was used to accomplish this [18]. Input values for the HyRAM models were determined from descriptions in literature sources. All of the input parameter values for all of the comparisons done are given in Appendix A.

Key outputs from each model were compared to the experimental results. For the blowdown model, the mass flow rate, pressure drop, and temperature in the tank as a function of time were compared. The plume/jet model predicts two-dimensional fields of velocity, mole/mass fractions, and temperatures. Experimental data is commonly plotted as centerline (or inverse centerline) mole/mass fraction and/or velocity, and radial profiles of mole/mass fraction and/or velocity. The HyRAM flame model predicts the trajectory and temperature of a flame, including the flame length. The radiant heat flux from a flame is also calculated by the flame model, which is a key parameter in estimating the risk from a hydrogen leak. Finally, the indoor accumulation and overpressure model predicts the concentration within a uniform layer at the ceiling of an enclosure as a function of time, along with the overpressure generated in the enclosure following ignition of that mixture. Each of these key parameters was compared to experimental data.

Comparisons were made between the "major versions" of HyRAM 2 and 3. The source code for both versions is available on the public GitHub repository for HyRAM. Specifically, version 2.0.0[1] was used for HyRAM 2 and version 3.1[2] was used for HyRAM 3.

[1] https://github.com/sandialabs/hyram/releases/tag/v2.0.0
[2] https://github.com/sandialabs/hyram/releases/tag/v3.1

This page intentionally left blank.

3. RESULTS AND DISCUSSION

This section shows a comparison of HyRAM 2.0 (which uses the Abel-Noble equation of state) with HyRAM 3.1 (which uses a real gas equation of state). Results from both versions of HyRAM are compared against experimental validation data in the literature in order to see the level of agreement. The following sub-sections include comparisons from multiple literature sources with different models within HyRAM, including blowdown/mass flow, unignited plumes, ignited jet fires, and accumulation/overpressure in an enclosure.

3.1. Blowdowns

A "blowdown" is the process of a pressure vessel emptying due to a leak or release. After the validation plots were identified and digitized, the input parameters for each table or figure was identified from each reference. Table 3-1 lists the tables and figures that were digitized and used as validation for the blowdown model.

Table 3-1 Blowdown Validation Data Sources

Author(s)	Year	Figure/Table Number
Ekoto et al. [19]	2012	Figure 3
Schefer et al. [20]	2007	Figure 4
Proust et al. [21]	2011	Figure 4
Schefer et al. [22]	2006	Figure 3b

Blowdown conditions described in the Ekoto et al. [19] paper included a hydrogen tank release with initial conditions: tank volume 3.63 L, tank pressure 13.45 MPa, tank temperature 297 K, hydrogen mass 0.00363 kg, release diameter 3.56 mm, and a discharge coefficient of 0.75. An apparatus was designed and constructed to mimic a hydrogen forklift release. The release enclosure was 34.3 cm long, 34.3 cm wide, and 43.5 cm high and elevated 6.4 cm off the facility floor. The release area within the enclosure was a 13.1 cm by 13.1 cm square. The release simulated a blowdown of commercial six-pack of hydrogen tanks. The full experimental setup is described in Section 3.4. A comparison to HyRAM is shown in Figure 3-1.

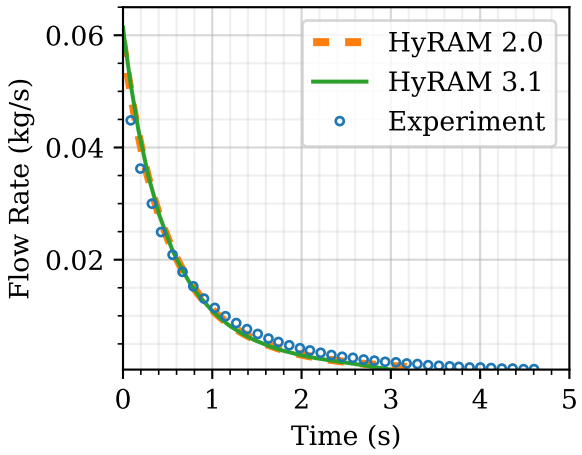

Figure 3-1 Flow rate data during blowdown from Ekoto et al. [19] compared to HyRAM models

The mass flow rate is plotted as a function of time. Both HyRAM 2.0 and HyRAM 3.1 predict similar initial flow rates of approximately 0.06 kg/s, with a blowdown time just over 3 seconds. The initial experimental data-point is approximately 0.45 kg/s, and the blowdown lasts nearly 5 seconds. Overall, the HyRAM predicted mass flow rates and blowdown time are similar to the experiment, with differences likely due to the assumption of isentropic flow from an adiabatic tank in HyRAM. Differences between HyRAM 2.0 and 3.1 predictions are minimal.

The experimental setup described by Schefer et al. [20] was designed to characterize high pressure, under-expanded hydrogen jet flames. Eight hydrogen tanks totaling 174.4 ft^3 contained a nominal pressure of 431 bar. Only two hydrogen tanks were used for the blowdown and three flame tests, the remaining six tanks remained closed. The exit diameter was 0.508 cm. Hydrogen was released vertically using a stagnation chamber. Cameras were used to measure the visible flame length, which were placed 14 and 15 meters away from the jet centerline. Radiometers were places around the flame to measure the radiative flux of the flame. The tank pressure as a function of time is shown in Figure 3-2. It should be noted that the data for the full figure and zoomed axis in Figure 3-2 appear to be different. This is because the source figure in Schefer et al. [20] from which the data is obtained do not clearly show data near a time of 0 seconds in the main figure, but the data are more clearly visible in the zoomed axis for the first 10 seconds of release.

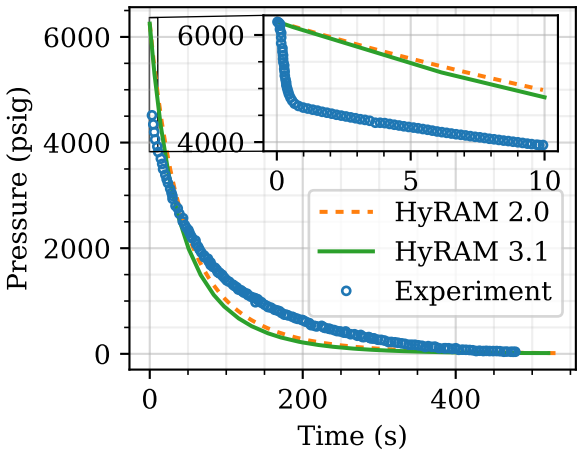

Figure 3-2 Pressure data during blowdown from Schefer et al. [20] compared to HyRAM models

As shown in the smaller zoomed axis of the first 10 seconds of the release, both HyRAM and the experiment start at approximately 6200 psig, but the experiment shows a rapid drop in pressure over the first 0.5 seconds to around 4500 psig, while the HyRAM pressure drop is more moderate. The authors [20] speculate that this initial rapid pressure drop is due to the flow entering the stagnation chamber, an aspect not caputred in the HyRAM model. Overall, both the experiment and HyRAM predict the blowdown to last for around 500 seconds, and have similar curves. The pressure drop predicted by HyRAM 2.0 is slightly slower than HyRAM 3.1, and lasts a few seconds longer, but overall, there is little difference between the models using the different equations of state and solution methods.

Proust et al. [21] performed experiments with a hydrogen tank reservoir with a 25 L volume with a varying release diameter between 1 mm and 3 mm. The hydrogen was released horizontally. A blowdown was reported with an initial pressure of 90 MPa through a 2 mm diameter orifice. The full experimental setup is described in Section 3.3. A comparison of the exprimental blowdown to the HyRAM models is shown in Figure 3-3.

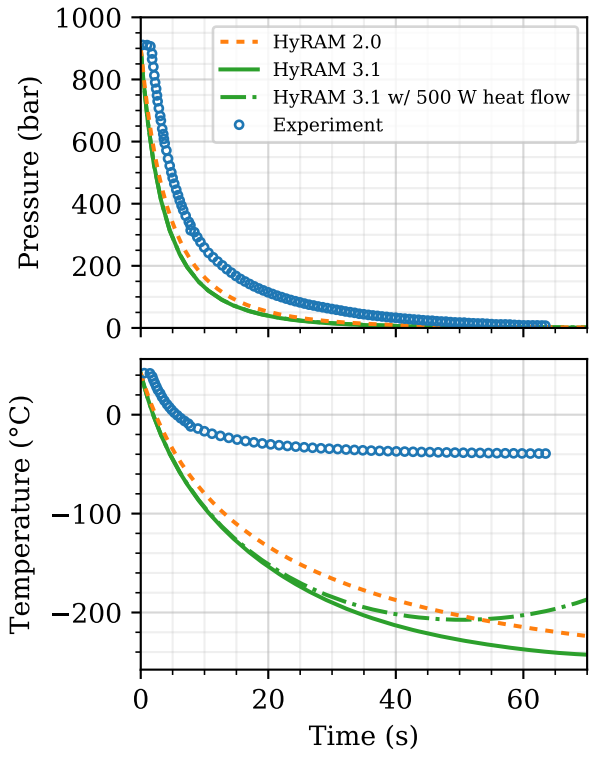

Figure 3-3 Tank pressures and temperatures during blowdown from Proust et al. [21] compared to HyRAM models

The experiment and models show the pressure dropping from 900 bar to atmospheric pressure over approximately 65 seconds, with both versions 2.0 and 3.1 of HyRAM predicting a faster initial pressure drop. The temperatures, shown in the bottom frame of Figure 3-3 predicted by HyRAM (minimum temperature below -200°C) are much lower than those measured experimentally (minimum temperature around -30°C). One reason for this discrepency could be the assumption that the tank is adiabatic. HyRAM 3.1 enables a heat flux to be specified into the tank. Even with a heat flux of 500 W into the tank (shown by the thick, dashed green line), the predicted tank temperatures are still well below those measured experimentally. The temperature was measured just upstream of the orifice, and it is possible that the gas in the reservoir is not well-mixed, which is an assumption made by HyRAM. There are small differences between HyRAM 2.0 and 3.1 predictions, with HyRAM 3.1 predicting a slightly faster initial pressure drop and a faster temperature decrease, but the models both predict a similar duration of the release. These differences between the data and predictions indicate that while HyRAM seems to be reasonably accurate for predicting mass flow rates and pressure histories during a blowdown, it is not accurate for predicting tank temperatures. Gas temperatures inside a tank during a blowdown are generally not used in risk or hazard assessments, so this is not expected to significantly affect hazard analyses.

Schefer et al. [22] report a tank blowdown starting at a total pressure of 2250 psia through a 3.175 mm orifice diameter. Other experimental details are included in Section 3.3. Comparisons of the blowdown to the different HyRAM versions are shown in Figure 3-4.

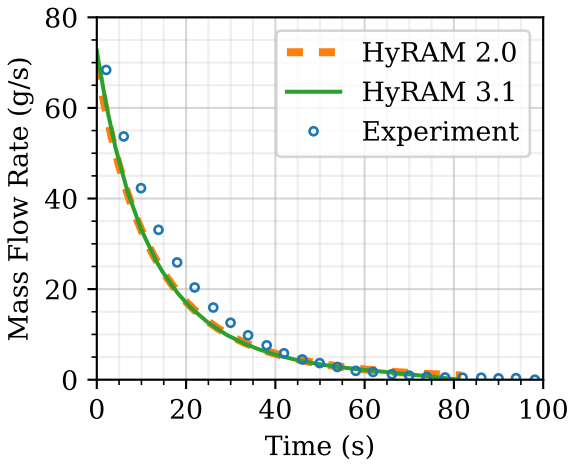

Figure 3-4 Mass flow rate data for a blowdown from Schefer et al. [22] compared to HyRAM predictions

The mass flow rates predicted by HyRAM are very similar to those reported in the paper, with the mass flow rate predicted by HyRAM decaying slightly faster initially than the experiment. There is very little difference between the two HyRAM versions, with both showing a blowdown duration of just over 80 s, while the experimental blowdown took around 100 s.

Overall HyRAM 2.0 and 3.1 predict very similar pressures, flow rates, and durations during tank blowdowns. Both versions of the blowdown model also predict flow rate and pressure histories similar to the experimental measurements. Neither version of the model is able to capture the tank temperatures that were experimentally measured by Proust et al. [21] likely due to the model assumption of a well-mixed, adiabatic (or constant heat flux) tank. It would require more complex modeling to accurately capture tank blowdown physics (i.e., computational fluid dynamics). The HyRAM models can be confidently used to predict pressure and mass flow histories during a blowdown.

3.2. Unignited Jet Plumes

Table 3-2 lists the tables and figures that were used as validation for the unignited jet model in HyRAM.

Table 3-2 Unignited Jet Validation Data Sources

Author(s)	Year	Figure/Table Number
Molkov [23]	2012	Table 5-3
Houf and Schefer [6]	2008	Figures 5, 8, 9
Ruggles and Ekoto [24]	2012	Figure 7
Han et al. [25]	2013	Figures 3, 6, 7, 8

Molkov [23] compiled data from experiments conducted by other researchers to assess the similarity law for expanded and under-expanded jets. A brief description of the original works are provided here; more details can be found in Section 5.3.3 of the book Fundamentals of Hydrogen Safety Engineering I by Molkov [23]. Six previous experiments were compared:

- Chaineaux et al. [26] conducted experiments to measure the axial concentration decay of hydrogen and methane horizontal jets. The tank volume was 0.12 m^3, initial pressure of 10 MPa, released at 2.2 m above the ground, with orifice diameters of 5 mm, 12 mm, and 24 mm for various tests.
- Kuznetsov [27] conducted experiments to analyze hydrogen distribution of horizontal jets inside a compartment of total volume of 160 m^3. The test initial pressures ranged from 2–26 MPa and orifice diameters ranging between 0.16 mm to 1 mm. A flow rate controller was used to keep a constant mass flow rate. Hydrogen concentration and flow velocity measurements were captured at 0.75 m, 1.5 m, and 2.25 m from the nozzle for eight different experimental setups.
- Okabayashi et al. [28] conducted five different experimental setups to measure the averaged volumetric concentrations of hydrogen along the jet. The releases were conducted horizontally 1 m above the ground, with various orifice diameters and pressures. The orifice diameters include 0.25 mm, 0.5 mm, and 1 mm at and initial pressure of 40 MPa. For the 2 mm release two initial pressures of 20 MPa and 40 MPa were used. Concentrations were captured at 4 m, 6 m, 8 m, 11 m, 15 m, 20 m, 30 m, and 50 m from the release point. All experimental data points from these experiments were not captured in Table 5-3 of Molkov's book [23]. This comparison uses the data points directly from Molkov [23], which include the minimum and maximum results for each experimental setup as well as intermediate results for the 1 mm and 2 mm orifices at 40 MPa.
- Ruffin et al. [29] conducted experiments measuring the axial concentration decay of sub-sonic hydrogen and methane jets. A 5 m^3 volume tank had an initial pressure of 4 MPa and an initial temperature of 288 K. Ruffin conducted four experiments with orifice diameters of 25 mm, 50 mm, 75 mm, and 100 mm. The data points were gathered at 2 seconds after the release and the pressure at 2 seconds were 1.79 MPa, 0.746 MPa, and 0.257 MPa.

- Shirvill et al. [30] conducted experiments for hydrogen concentration with a high pressure system at 17.3 MPa. The experiments were conducted with discharge pressures of 1.1–15.1 MPa and orifice diameters of 1–12 mm. The releases were conducted horizontally at 1.5 m above the ground. Hydrogen concentrations were gathered at 1.0 m, 1.5 m, and 2.0 m along the jet, with the maximum and minimum values being included in Table 5-3 of Molkov.
- Veser et al. [31] conducted experiments to determine the hydrogen distribution of horizontal hydrogen jets, with orifice diameters of 1 mm, 2 mm, or 4 mm and a range of initial pressures between 0.5 MPa and 6.0 MPa, released at 0.9 m above the ground. Gas was released at temperatures of 35 K, 65 K, 80 K, and 298 K, and the temperature and concentration were measured along the jet.

The centerline mass fractions reported by Molkov [23], based off of different literature experiments, are shown in Figure 3-5. It can be difficult to see in Figure 3-5, but it is worth noting that for cases in which experimental data exists at temperature below 150 K (Veser et al. [31]), HyRAM 3.1 predictions are shown but HyRAM 2.0 predictions are not due to the fact that HyRAM 2.0 is not in a valid temperature range. It should also be noted that for some sub-figures in Figure 3-5, the solid lines for HyRAM 3.1 overlap, making them difficult to distinguish.

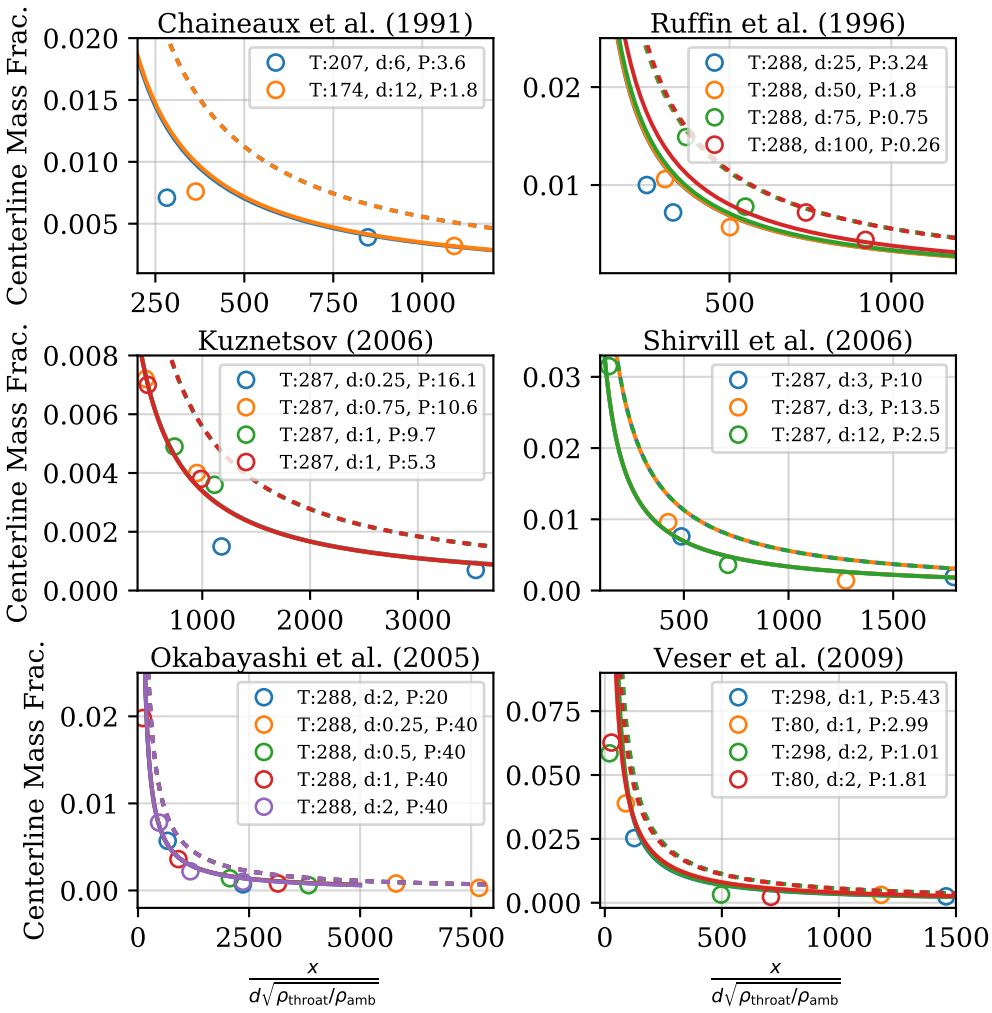

Figure 3-5 Centerline mass fractions from data compiled by Molkov [23]. In the legends, T denotes temperature (K), d denotes diameter (mm), and P denotes pressure (MPa). Lines are results from HyRAM, with the same colors as the conditions in the legends. The dashed lines are from HyRAM 2.0 while the solid lines are from HyRAM 3.1.

The temperature of these releases spans from 80 K to 288 K, with pressures from 1 MPa to 40 MPa. HyRAM 2.0 tends to predict slightly larger centerline mass fractions at all normalized distances. Both models agree with the data well, with HyRAM 2.0 tending to slightly overpredict the mass fraction at all normalized distances. HyRAM 3.1 slightly underpredicts the centerline mass fractions for some of the Ruffin et al. [29] and Kuznetsov [27] data. Differences in concentration are primarily due to an update to momentum driven entrainment in HyRAM 3.1 over HyRAM 2.0. HyRAM 3.1 uses the conditions at the notional nozzle to calculate momentum driven entrainment, while HyRAM 2.0 uses the conditions at the true orifice [4].

Houf and Schefer [6] designed an experiment to measure the leak rate, buoyant jet shape, and concentration field for slow leaks. A planar laser-Rayleigh scattering diagnostic was used to measure hydrogen leak flow. The leak diameter of 1.905 mm was used and the hydrogen was released vertically. The flow conditions were at ambient room conditions temperature and

pressure of 294 K and 100 kPa. Figure 3-6 shows a comparison of mass fraction cross-sections at various normalized downstream distances.

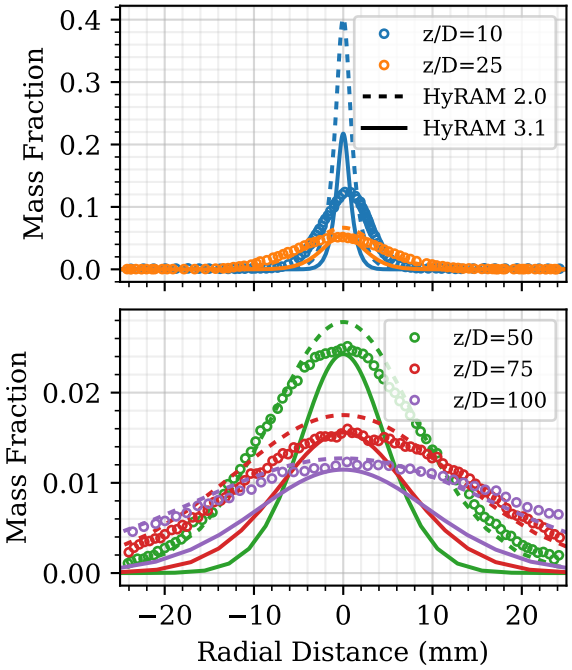

Figure 3-6 Radial profiles of mass fraction at several downstream locations reported by Houf and Schefer [6] (symbols) compared to HyRAM 2.0 and 3.1 (lines)

At a downstream location of $z/D = 10$, both HyRAM 3.1 and 2.0 overpredict the centerline mass fraction significantly, with HyRAM 2.0 predicting much higher centerline mass fractions than HyRAM 3.1. For greater downstream distances in both the top and bottom frames, the centerline mass fractions are much closer to the experimentally measured values. HyRAM 2.0 predicts higher centerline mass fractions at all downstream distances, HyRAM 3.1 matches the centerline pretty well for $z/D \geq 25$.

HyRAM 2.0 matches the radial profile data better than HyRAM 3.1 for axial distances of 25 or more diameters downstream in Figure 3-6. The predictions of the mass fraction profile for HyRAM 2.0 are wider than for HyRAM 3.1 at all downstream distances. The differences in entrainment discussed previously between HyRAM versions would not affect the low-pressure releases of Figure 3-6. Rather, the differences in profiles here are primarily due to the fact that the relative velocity to scalar ratio in HyRAM 2.0 is higher (1.5) than for HyRAM 3.1 (1.16). Predictions for radial profiles could be improved with better tuning of the empirical parameters in the HyRAM models, for entrainment and spreading ratio, but this still needs to be explored.

Centerline inverse mole fractions are shown as a function of distance, for a Froude number of 268 in Figure 3-7a. Similar to the radial profiles in Figure 3-6, the centerline concentrations are overpredicted (lower inverse mass fractions) at small axial distances, and the centerline concentration agreement is much better at further distances. It is clear in Figure 3-7a that HyRAM 3.1 is closer to the experimental data than HyRAM 2.0 at higher axial distances.

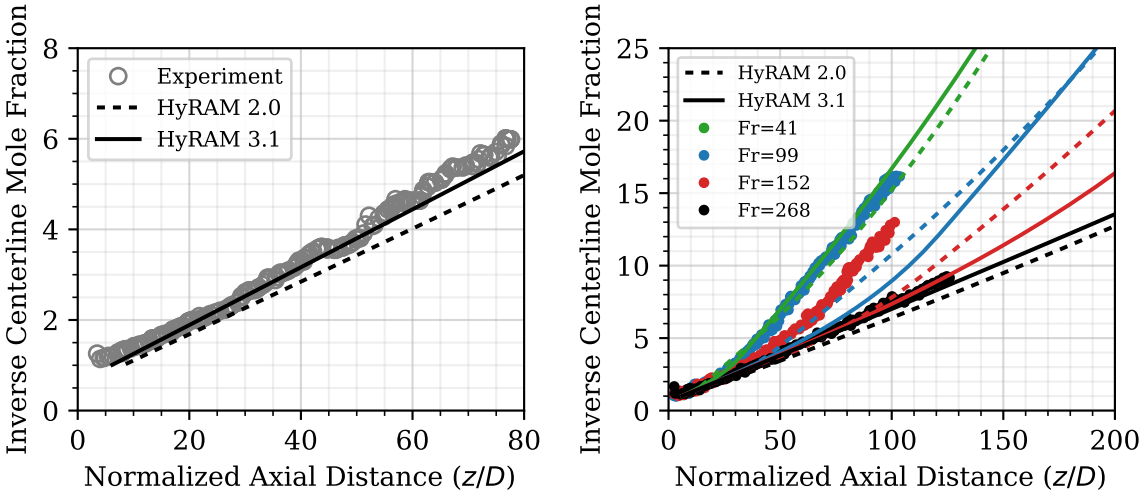

(a) Zoomed view for a densimetric Froude number of 268

(b) Several densimetric Froude numbers

Figure 3-7 Inverse centerline mole fraction as a function of downstream distance as reported by Houf and Schefer [6] (symbols) and predicted by HyRAM (lines)

In Figure 3-7b, inverse centerline mole fractions for a Froude number of 268, as well as several lower Froude numbers are shown. In the case of the smaller Froude numbers, buoyancy begins to play a role in the decay of the centerline concentration. While Houf and Schefer [6] report that the data is for Froude numbers of 99, 152, and 268, we suspect that Figure 9 in their work may have been mislabeled, as the paper also discusses releases with a smaller Froude number of 41. The HyRAM simulations (both versions 2.0 and 3.1) for the Froude number of 41 agree well with the data reported as for a Froude number of 99, which is buoyancy dominated, with a higher slope of the inverse mole fraction, for near distances to the release point. The higher Froude number releases transition from momentum dominated (small slope) to buoyancy dominated (higher slope) at various distances downstream. HyRAM 2.0 begins to predict the deviation from a momentum to buoyancy dominated release closer to the release point, but as is clear for the simulations for a Froude number of 99, both HyRAM versions predict similar concentration decay both near and far from the release point. Additional buoyancy-affected release data is needed to assess whether the transition to buoyancy affected releases is being properly predicted, or whether the data in the Houf and Schefer [6] paper was mislabeled.

Experiments by Ruggles and Ekoto [24] were designed to investigate the flammability factor concept to predict ignition boundaries for releases from compressed bulk hydrogen leaks. The team designed and integrated a high-pressure stagnation chamber to produce pressure ratios up to 60:1 to investigate under-expanded hydrogen jets. Dynamic feedback was used to maintain a steady pressure ratio throughout the tests of 10:1 (stagnation to ambient pressure). The experimental conditions of the stagnation chamber were a 0.75 mm release radius, a pressure of 983.2 kPa, a temperature of 295.4 K, a density of 0.796 kg/m^3, and a 0.979 discharge coefficient. The atmospheric conditions were 296 K and 98.37 kPa. Figure 3-8 shows the inverse centerline mass fraction and the jet half-width as a function of normalized distance.

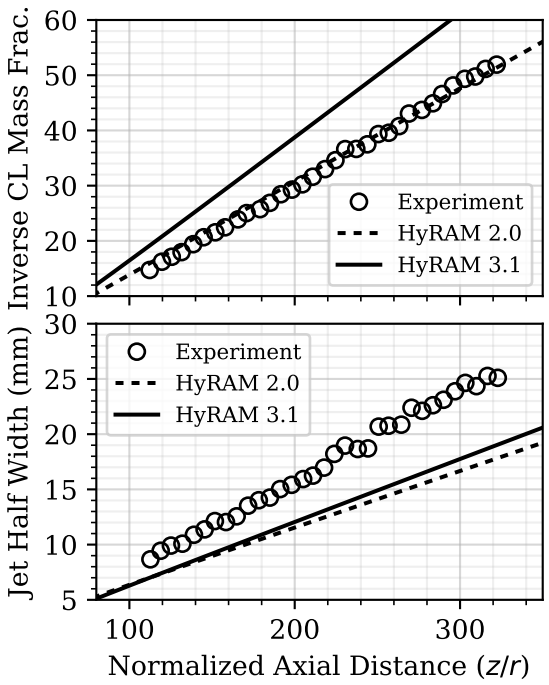

Figure 3-8 Inverse centerline mass fraction and half-width as a function of normalized downstream distance from Ruggles and Ekoto [24] compared to HyRAM 2.0 (dashed lines) and HyRAM 3.1 (solid lines)

As with the previous simulations, HyRAM 3.1 predicts a lower centerline mass fraction (higher inverse centerline mass fraction) than HyRAM 2.0 at all distances. For these high pressure jets, HyRAM 3.1 tends to underpredict the inverse centerline mass fraction, while HyRAM 2.0 agrees well with the data. The jet half-width is the distance to the point where the mass fraction is half of the centerline value; this value increases as a function of downstream distance as air is entrained into the flow. HyRAM 3.1 predicts a slightly wider half-width than HyRAM 2.0 at all downstream locations, but both versions of HyRAM are predicting thinner profiles than the data.

Han, Chang, and Kim [25] investigated the concentration distribution of hydrogen leaking from high pressure sources with leak diameters smaller than 1.0 mm. Hydrogen concentrations were measured at several distances for various exit diameters and pressures. The hydrogen concentrations were measured at 1 m, 3 m, 5 m, 7 m, and 9 m away from the jet exit. This was done for the permutations of initial tank pressures of 100 bar, 200 bar, 300 bar, and 400 bar and exit diameters of 0.5 mm, 0.7 mm, and 1.0 mm. Figure 3-9a shows the centerline mole fraction as a function of downstream distance.

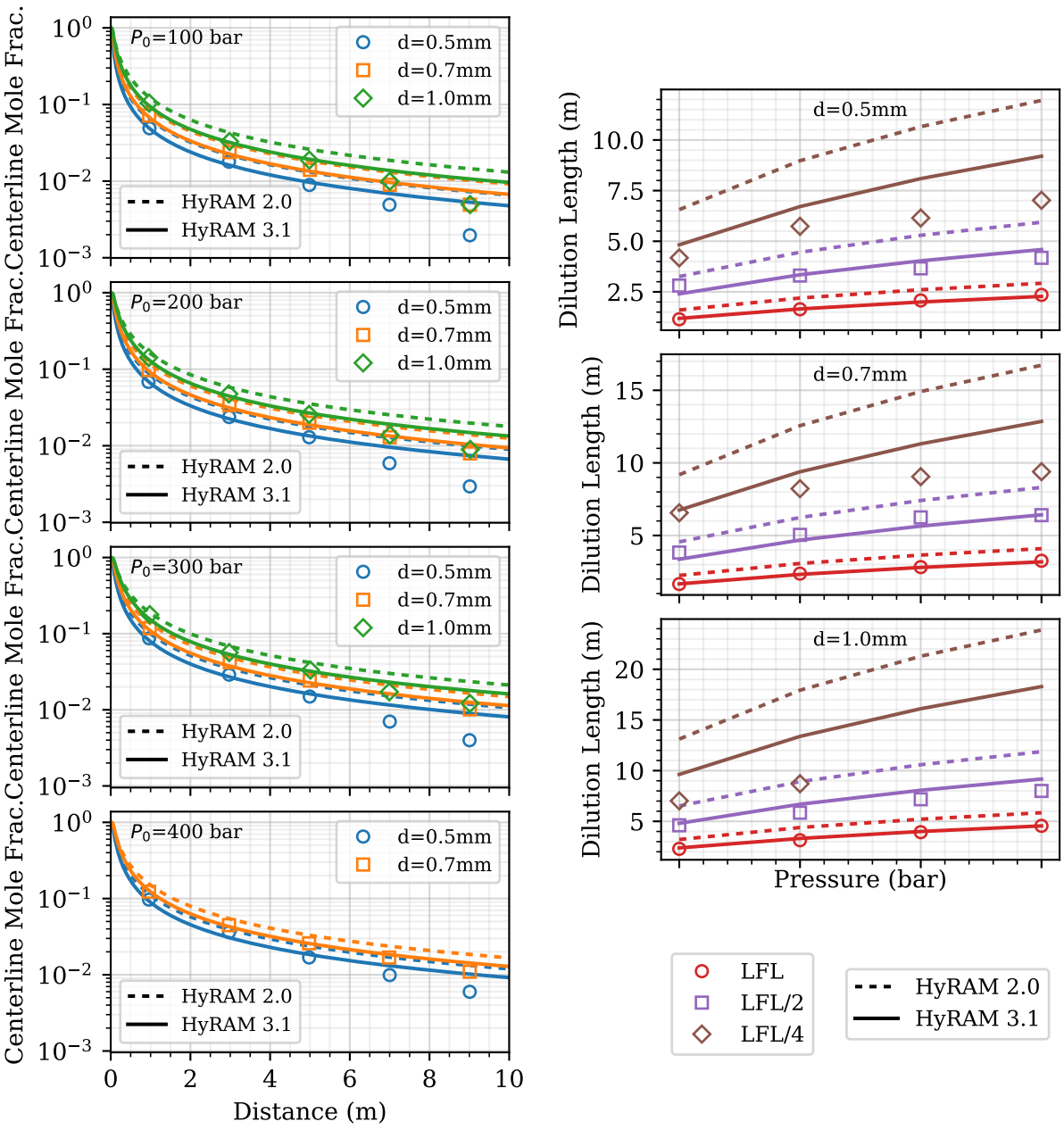

(a) Centerline mole fractions

(b) Dilution length (centerline distance to fraction of LFL)

Figure 3-9 Data for 100–400 bar jets, as reported by Han et al. [25] compared to HyRAM

As was the case previously, HyRAM 2.0 (dashed lines) predicts higher centerline mole fractions than HyRAM 3.1, in all cases. On the log-scale it is a bit difficult to assess the absolute accuracy, but the HyRAM 2.0 lines tend to be at the top edge of the symbols (indicating overprediction), while the HyRAM 3.1 predictions are more centered on the data-points. Both models overpredict the concentrations at large axial distances. The dilution length is the distance to a certain fraction of the flammability limit, which is critical to safety, and shown in Figure 3-9b. This figure makes

it easier to assess the amount of overprediction in mole fraction for low concentrations. HyRAM 3.1 shows good agreement with the distances measured experimentally for all of the conditions shown for the lower flammability limit (LFL) (mole fraction of 0.04 for hydrogen) and half of the LFL, while HyRAM 2.0 slightly overpredicts these distances. Both versions of HyRAM overpredict the dilution length for 1/4 of the LFL (mole fraction of 0.01).

Figure 3-10 provides another comparison of the centerline mole fractions measured by Han et al. [25] for the high pressure hydrogen jets.

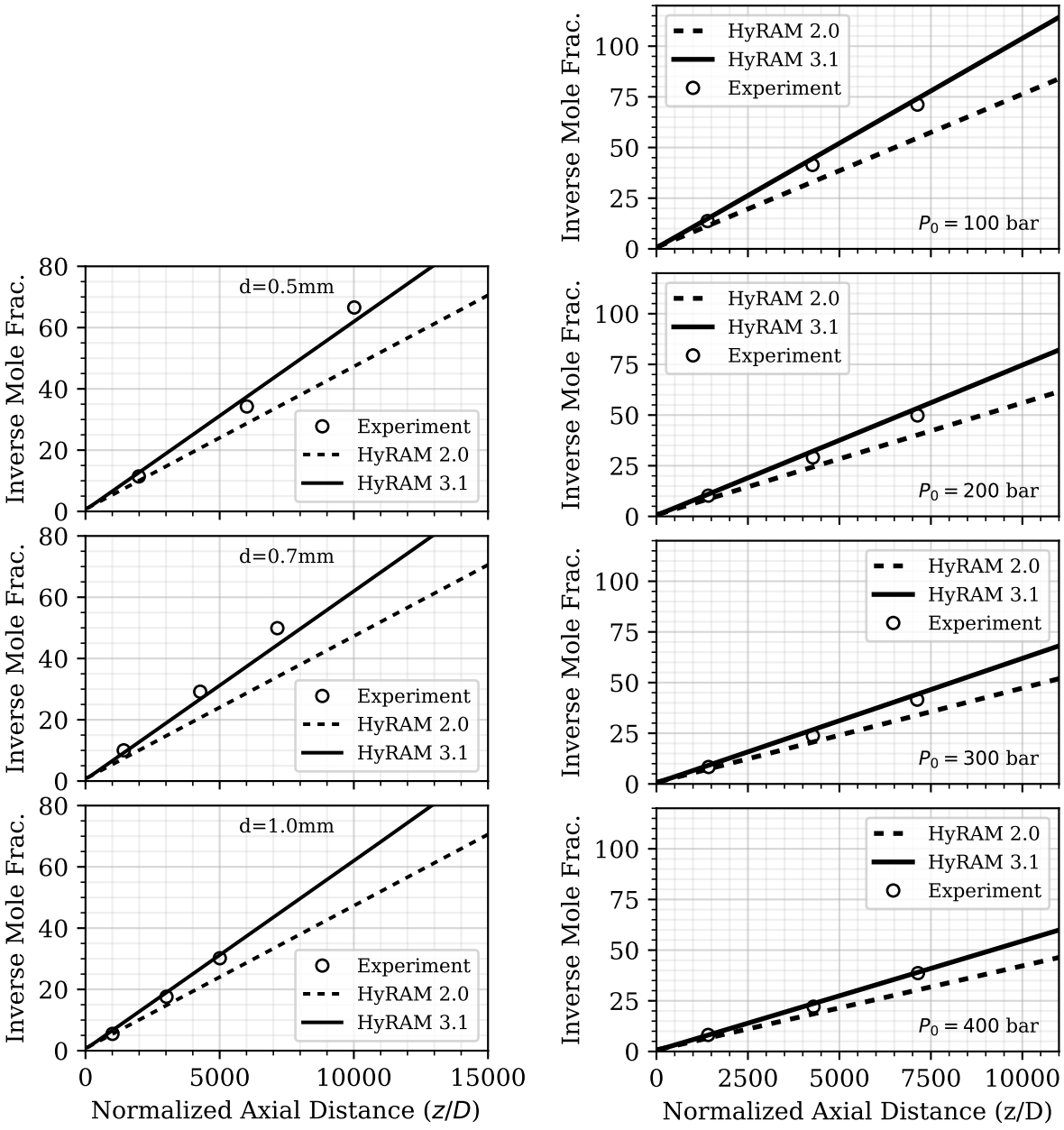

(a) Different diameters for a pressure of 300 bar

(b) Different pressures for a 0.7 mm nozzle

Figure 3-10 Inverse centerline mole fraction as reported by Han et al. [25] compared to HyRAM

Both groupings of the data show that HyRAM 2.0 tends to overpredict the mole fraction (or underpredict the inverse mole fraction). HyRAM 3.1 agrees with the data very well, predicting the magnitude and linear slope of the inverse mole fraction as a function of normalized axial distance.

Overall, both HyRAM 2.0 and 3.1 can predict unignited centerline concentrations well for the data given, while also capturing buoyancy effects. HyRAM 2.0 predicts higher centerline concentrations for a given set of conditions than HyRAM 3.1, primarily due to the increased momentum driven entrainment in HyRAM 3.1. This results in more accurate and less conservative predictions of dilution lengths for HyRAM 3.1. Both models predict radial profiles that are not as wide as those measured experimentally. Potential model parameters that could lead to improved predictions are the relative velocity to mass-fraction spreading ratio, empirical constants within the entrainment models, or adjustment of the notional nozzle model physics.

3.3. Ignited Jet Fires

Table 3-3 lists the tables and figures that were used as validation for the HyRAM flame model.

Table 3-3 Flame Validation Data Sources

Author(s)	Year	Figure/Table Number
Ekoto et al. [10]	2014	Table 2
Schefer et al. [22]	2006	Figure 8
Houf and Schefer [9]	2007	Figures 5, 6
Imamura et al. [32]	2008	Table 2
Mogi et al. [33]	2005	Figure 9
Proust et al. [21]	2011	Figures 8, 10

Ekoto et al. [10] performed experiments measuring the length and heat flux from two large scale jet flames. The experiments were conducted outside using compressed hydrogen at 60 bar_g stagnation pressure released horizontally. The two tests were conducted with orifice diameters of 20.9 mm and 52.5 mm. Full boundary conditions are provided in Table 1 in the paper. Two cameras were used to measure the visible flame lengths and a radiometer measure the heat flux at a single location for each flame. The experimental results were compared to various notional nozzle models in Table 2 of the paper based on flame length and the radiative heat flux for both straight and curved flames. Experimental results are compared to HyRAM predictions in Table 3-4.

Table 3-4 Flame Length and Heat Flux Results from Ekoto et al. [10] compared to HyRAM

$d_{orifice}$	Length [m]			Heat Flux [kW/m^2]		
[mm]	Measured	HyRAM 2.0	HyRAM 3.1	Measured	HyRAM 2.0	HyRAM 3.1
20.9	17.4	19.7	19.9	4.7	6.4	6.3
52.5	45.9	47.3	47.7	23.9	36.1	27.2

As shown, the flame lengths predicted by HyRAM 2.0 are very similar to HyRAM 3.1, with both versions of the software overpredicting the measured visible flame length. The heat flux values for HyRAM 2.0 are larger than for HyRAM 3.1; pretty significantly for the larger flame. In all cases, HyRAM predicts a higher heat flux than was measured experimentally.

The experimental setup for the Schefer et al. [22] paper was designed to measure the flame length of a high pressure hydrogen leak ignited at the source. Six high pressure hydrogen cylinders were used with an average pressure of 2250 psi_a per full cylinder. Only two cylinders were used for the tests with a vertical release and a 3.175 mm orifice diameter, which flowed through a 7.94 mm tube which sustained the flame. A tank blowdown starting at a total pressure of 2250 psi_a was conducted to identify the mass flow rate of the release. To measure the flame length, the infrared and ultraviolet spectrum was captured to characterize the structure, length, and width of the flame.

The radiative flux was measured using thermopile detectors both along the flame and at perpendicular radial distances. It should be noted that in this paper [22], the radial distance of the radiometers is reported as half the visible flame length, while in a subsequent paper [9], the radial distance is reported as 1.82 m. In these HyRAM simulations, we assumed that the radial distance of the radiometers was 1.82 m, as the visible flame length is not clearly defined for a blowdown (we assume that the authors did not move the radiometers to a set location for each of the times in the blowdown that were reported), and using half of the visible flame length at each time reported gave heat fluxes that were very different from the measurements.

Figure 3-11 shows measurements of heat flux at different distances away from the leak point (normalized to visible flame length) for different times and compares these to HyRAM predictions.

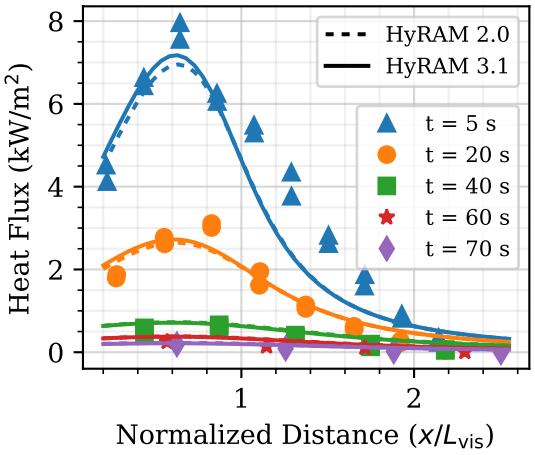

Figure 3-11 Heat flux during a blowdown as reported by Schefer et al. [22] (symbols) and predicted by HyRAM (lines)

As would be expected, the heat flux decreases as the pressure in the tank reduces (longer times). This is captured by both the simulations and the experimental data. Both the experiments and simulations predict similar shapes of the heat flux along the flame length, with a peak in heat flux around 70% of the visible flame length. HyRAM 3.1 predicts slightly higher heat fluxes than HyRAM 2.0, and the peak heat flux and drop-off at radiometer distances above 70% of the visible flame length happens faster than the experimental measurements, particularly for the data 5 seconds after the start of the release. HyRAM predictions match the heat flux measurements well for 20–70 seconds after the release.

In a subsequent paper, Houf and Schefer [9] reported additional data (flame lengths and heat fluxes) from their previous experimental campaign [22]. Figure 3-12 shows the flame length as a function of time and the radiation heat flux at different distances (normalized by visible flame length) as compared to HyRAM predictions.

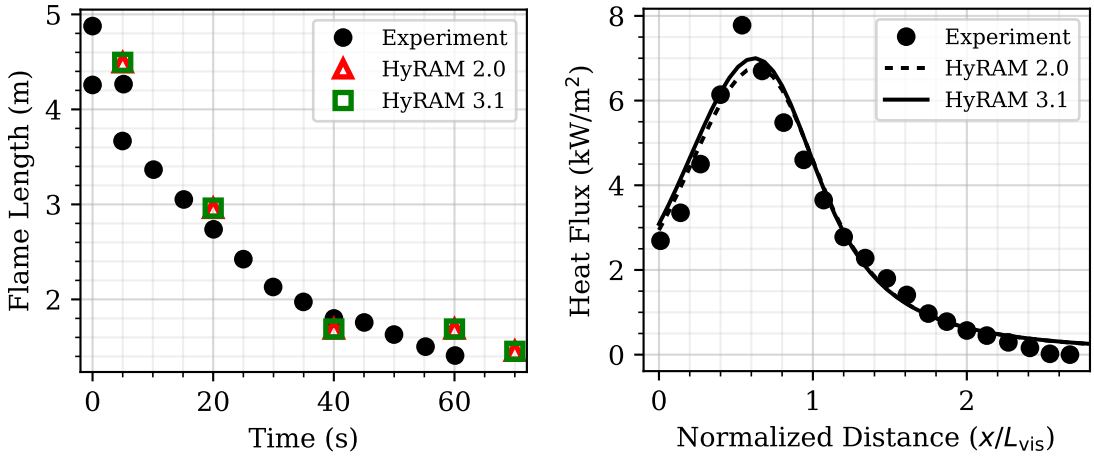

(a) Flame length over time

(b) Radiative heat flux vs. axial distance 5 seconds into the release

Figure 3-12 Data from Houf and Schefer [9] compared to HyRAM

As shown in Figure 3-12a, the flame lengths predicted by HyRAM 2.0 and 3.1 are almost exactly the same. These flame lengths are slightly longer than the measured flame lengths. The decay of the flame length is accurately captured, although it should be noted that the flames were simulated, based on the mass flow rate and jet velocities reported in the paper [22] rather than the blowdown model of HyRAM. Figure 3-12b is similar to Figure 3-11, although the experimentally reported heat fluxes in this paper [9] drop off faster at larger axial distances than was reported previously [22] at 5 seconds. In these simulations, both versions of HyRAM agree with the data very well along the length of the flame, although both versions predict peak heat fluxes slightly below those measured experimentally.

Imamura et al. [32] measured the flame shape and temperature profiles for a range of hydrogen flames. A hydrogen spouting system was used with a regulator and measurements of the pressure near the nozzle. Four nozzle diameters of 1–4 mm were used at spouting pressures of 0.5–3.0 MPa. Figure 3-13a shows the measured mass flow rates at different spouting pressures and nozzle diameters compared to HyRAM predictions.

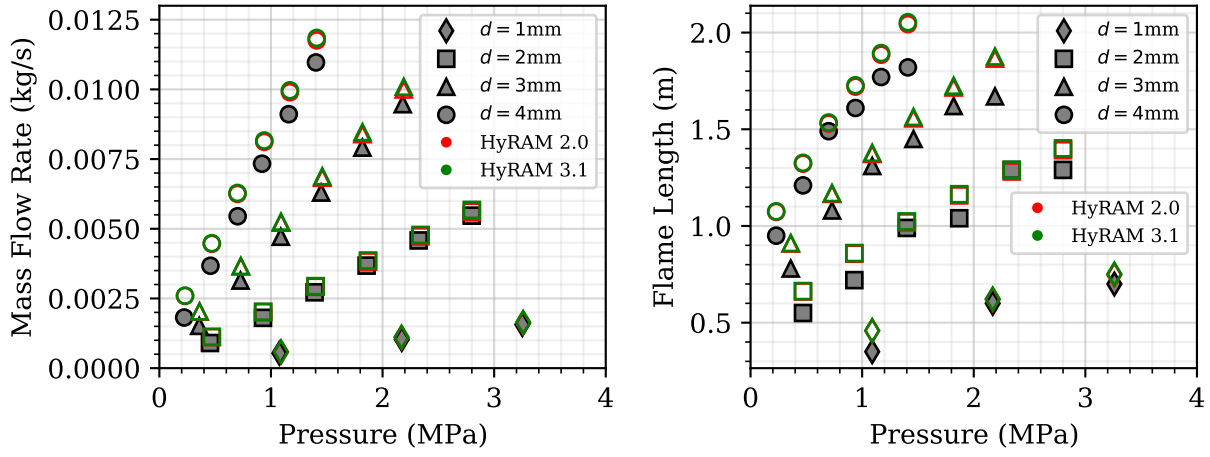

(a) Mass flow rates

(b) Flame lengths

Figure 3-13 HyRAM comparisons to data from Imamura et al. [32]

The HyRAM mass flow rates, calculated using the measured pressures, are slightly higher than those reported experimentally. With these pressures, and ambient temperatures, both versions of HyRAM predict nearly identical mass flow rates through the orifices. Using the HyRAM calculated mass flow rates, the flame lengths of these ignited releases were calculated. Figure 3-13b shows flame length measurements for the different spouting pressures and nozzle diameters as compared to HyRAM predictions. The flame lengths from HyRAM 2.0 and 3.1 are nearly identical, much like the mass flow rates. The flame lengths predicted by HyRAM are slightly longer than the experimental measurements, especially for the longest flame lengths. Some of this error is due to challenges in defining and measuring the visible flame length.

The shape and radiative heat flux of high pressure hydrogen jet flames were measured by Mogi et al. [33]. The experimental setup included high pressure hydrogen cylinders with a maximum pressure of 45 MPa and a total capacity of 0.184 m^3. Flame lengths and widths were measured at various spouting pressures ranging between 0.01 MPa and 40 MPa for orifice diameters ranging between 0.4 mm and 4 mm. Flame lengths were also measured at various orifice diameters between 1–5 mm at different spouting pressures of 10 MPa, 20 MPa, and 35 MPa. Figure 3-14 shows heat flux measurements for various orifice diameters and distances away from the flame against different mass flow rates.

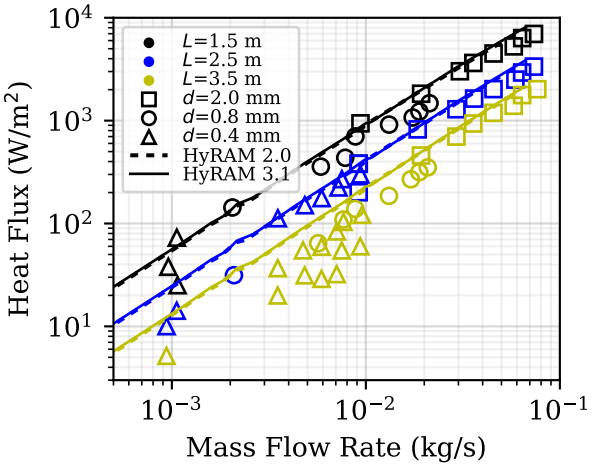

Figure 3-14 Radiative heat flux values for different mass flowrates from Mogi et al. [33] compared to HyRAM, in which d is the diameter of the orifice and L is the distance between the detector and flame axis

Intuitively, as the distance from the flame axis (L) becomes larger, the heat flux decreases, and the smallest diameter nozzles lead to the lowest mass flow rates and heat fluxes. HyRAM 2.0 and 3.1 predict nearly identical heat fluxes for the range of conditions in this study, and the predictions capture the experimental trends well. Some of the heat fluxes are overpredicted, particularly at low mass flow rates. HyRAM tends to give a conservative prediction for heat flux (i.e., the risk of harm from heat flux increases with increased heat flux).

Proust et al. [21] measured hydrogen flame characteristics of high pressure releases. The experiments measured pressure, temperature, and mass flow over the release duration. The hydrogen tank reservoir had a 25 L volume with a varying release diameter between 1–3 mm. The hydrogen was released horizontally. To measure the pressure during the release,a piezoresistive sensor was placed on the head of the bottle. To capture the flame temperature, ten thermocouples were placed along the line of the flame. The heat flux was measured by placing five fluxmeters at a 45°-angle horizontal to the flame. Figure 3-15a shows the flame length vs. pressure for the different release orifice diameters.

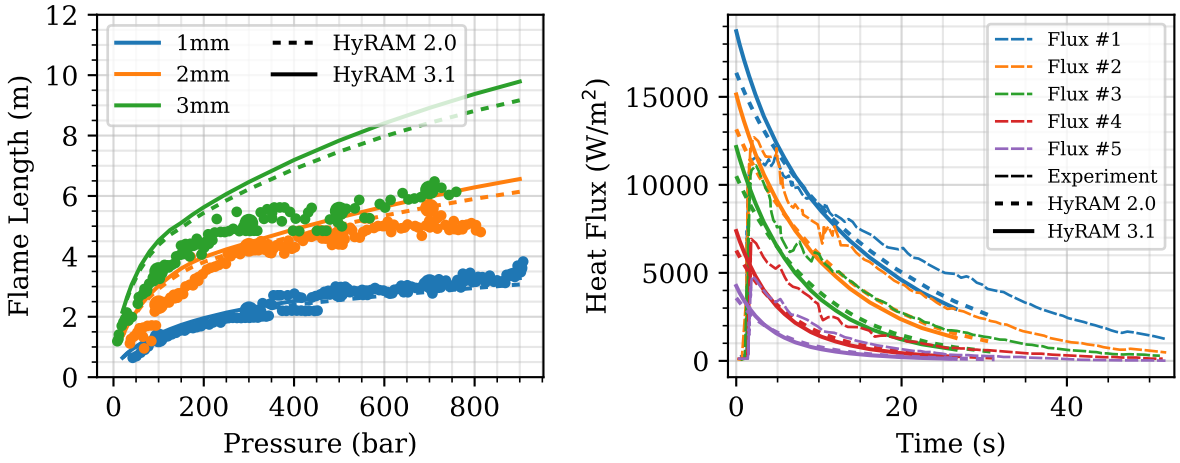

(a) Flame length vs. pressure

(b) Heat flux over time for a 2 mm orifice

Figure 3-15 HyRAM simulations compared to data from from Proust et al. [21] during a 900 bar blowdown

Once again, the flame lengths predicted by HyRAM 2.0 and 3.1 are fairly close, although at the highest pressures the discrepancy becomes more noticeable. As expected, the flame lengths are smaller for smaller pressures and for smaller diameter orifices. The HyRAM predictions agree with the data for the 1 mm and 2 mm orifices, but overpredict flame lengths pretty substantially for the 3 mm orifice, especially at the highest pressures. The authors explain that the flame lengths were extracted from video records, but do not completely describe the setup or criteria [21]. It is possible that the larger flames, with more luminous output, changed the f-number of the camera system, hence changing the criteria for the definition of length. It is also possible that the width—which in HyRAM is set to be 0.17 times the length—increases for the larger flames; there are significantly more combustion products for the 3 mm orifice than the 2 mm orifice at the highest pressure, but a modest experimental increase in flame length. While the HyRAM models could be improved to give more accurate results, the overprediction of flame length means that HyRAM deviates from the data in a conservative direction; hazard or risk assessments using this flame length at larger diameters and higher pressures would end up with a more conservative (longer) flame length than in reality.

The time history of the heat flux for the 2 mm blowdown is shown in Figure 3-15b. As expected, at the start of the blowdown when the pressure is the highest, the heat flux is the highest. Both HyRAM 2.0 and 3.1 have similar decreases in heat flux over time, with HyRAM 3.1 initially predicting higher heat fluxes, but HyRAM 2.0 eventually predicting slightly higher heat fluxes towards the end of the release. Experimentally, it takes some time for the radiometers to register the heat flux, but after they begin to register the heat flux, they show a similar decay and magnitude as the HyRAM predictions. HyRAM does overpredict at the beginning of the blowdown and underpredict toward the end of the blowdown, but this can at least partially be attributed to the thermal capacitance of the radiometers (they take time to register, and then time to decay).

Overall, HyRAM provides accurate predictions of flame length and heat flux, from hydrogen

flames up to 900 bar. HyRAM 2.0 and 3.1 provide nearly identical predictions of both flame length and heat flux, for the range of conditions in the literature.

3.4. Accumulation and Overpressure in Enclosures

Table 3-5 lists the tables and figures that were used as validation for the indoor accumulation and overpressure model in HyRAM.

Table 3-5 Overpressure/Accumulation Validation Data Sources

Author(s)	Year	Figure/Table Number
Ekoto et al. [19]	2012	Figures 9, 14
Giannissi et al. [34]	2015	Figure 7
Merilo et al. [35]	2011	Figures 2, 6a
Bernard-Michel and Houssin-Agbomson [36]	2017	Figures 7, 9

Ekoto et al. [19] performed experiments to study the overpressure in warehouse facilities. The experimental facility was 3.64 m wide, 4.59 m long, and 2.72 m tall with a total volume of 45.4 m^3. Hydrogen was released from a tank with a volume of 3.63 L, a pressure of 13.45 MPa, and a temperature of 297 K. This resulted in a hydrogen mass of 0.00363 kg, which was released through an opening with a diameter of 3.56 mm and a discharge coefficient of 0.75. To mimic a hydrogen release from a forklift, an apparatus was designed to replicate different release conditions. The release enclosure was 34.3 cm long, 34.3 cm wide, and 43.5 cm high, and elevated 6.4 cm off the facility floor. The release area within the enclosure was a 13.1 cm by 13.1 cm square. The release consisted of a blowdown of commercial six-pack of hydrogen tanks. The release enclosure was set towards the center and along the wall of the facility, while thermocouples and pressure sensors were placed across the facility. Various tests were done with and without a ventilation area, no ventilation, natural ventilation, and forced ventilation. Ignition locations and ignition times varied as well for the thirteen tests measuring hydrogen concentration over time at various locations within the facility and over-pressure values within the facility over time. Figure 3-16 shows the hydrogen mole fraction over time for three different sensors along the ceiling for tests with and without mechanical ventilation, with data reported by Ekoto et al. [19] compared to the HyRAM layer mole fraction predictions.

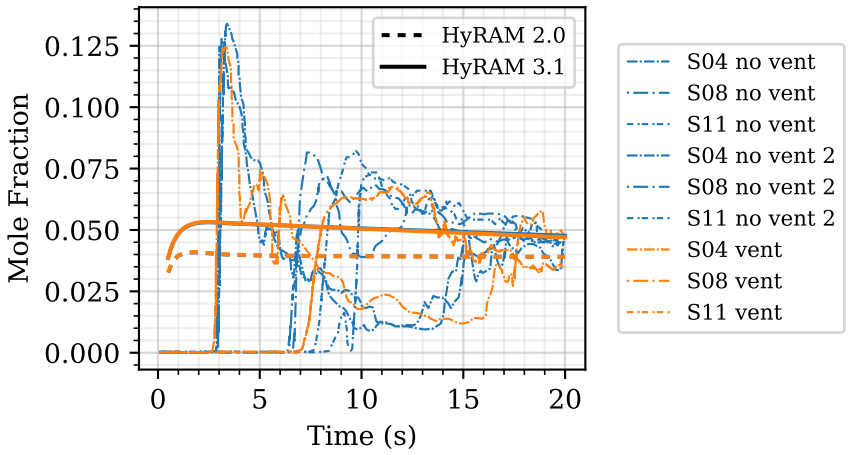

Figure 3-16 Hydrogen mole fraction measurements from different sensors at the ceiling over multiple experiments with and without ventilation from Ekoto et al. [19] compared to HyRAM predictions

For both versions of HyRAM, the mole fraction predictions are very similar for the tests both with and without ventilation. This result is similar to the experimental data, where the thin dashed orange and thin dashed blue lines have only minor differences in their readings. The predicted mole fractions of HyRAM 2.0 are below the predicted mole fractions for HyRAM 3.1 throughout the 20 seconds. The experimental data takes longer to achieve any concentration reading, and when the concentration registers with each sensor, there is a peak and then a decrease with significant fluctuations. These fluctuations in the experimental measurements are likely due to the turbulence and unsteadiness within the enclosure. The near steady-state (slightly decreasing) mole fraction predicted by HyRAM 3.1 is near the average of the sensor data while the prediction by HyRAM 2.0 appears to be a bit below the average.

The overpressures when Ekoto et al. [19] ignited the mixtures in the warehouse is shown in Figure 3-17.

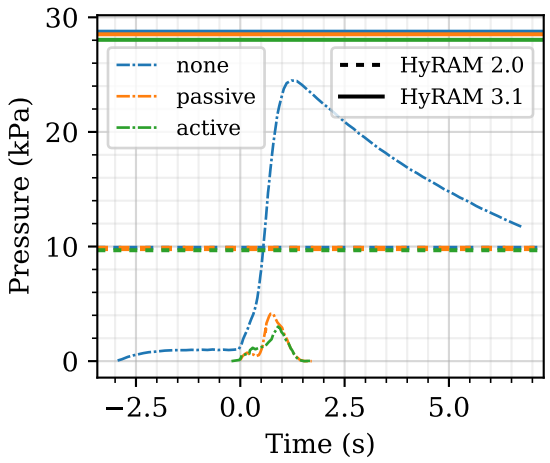

Figure 3-17 Overpressure values from Ekoto et al. [19] (thin, dashed lines) for igniting hydrogen mixtures 3 seconds after the start of the release (time of 0 is at the ignition time). Labels with respect to the colors relate to the ventilation, and HyRAM lines (thick) are the overpressure predictions for ignition after 3 seconds under the conditions described.

The authors ignited each of these releases after 3 seconds, looking at the effect of ventilation in this case. As shown, when there was no ventilation, the highest overpressure was achieved, registering on the pressure transducer just over 1 second after ignition. A slightly lower delay before peak overpressure was observed for the cases with passive and active ventilation, with peak overpressures significantly lower than the case with no ventilation. Also shown on this plot as the thicker, horizontal lines are the HyRAM 2.0 and 3.1 results for the pressure that would result after accumulating the gas mixture in the enclosure for 3 seconds. The HyRAM 3.1 pressures predicted are a little above the peak overpressure observed experimentally with no ventilation, and well above the peak ovepressures when there was ventilation. HyRAM 3.1 predicts the highest overpressure without ventilation, and slightly lower overpressures with passive and then active ventilation. HyRAM 2.0 predicts lower peak overpressures than HyRAM 3.1, and the difference between the cases with and without ventilation are even less than the differences shown by HyRAM 3.1 HyRAM 3.1 gives a conservative result relative to all of the experimental measurements, while HyRAM 2.0 gives a lower overpressure prediction than experimentally measured for the case without ventilation.

Giannissi et al. [34] describe some of the HyIndoor tests with measurements of the diffusion of hydrogen in a ventilated enclosure under various conditions. The test facility was a rectangular prism with a total volume of 31.25 m^3. Various release rates, wind conditions, and vent locations were tested. Twenty-seven oxygen sensors were placed within the facility to measure the hydrogen concentration for each of the different tests. They were placed on vertical planes to gather information on both horizontal and vertical flow. The hydrogen was released vertically from the center of the facility to measure the hydrogen concentration over time. Figure 3-18 shows the hydrogen concentration over time measured by three applicable sensors along the ceiling, as compared to the HyRAM predictions.

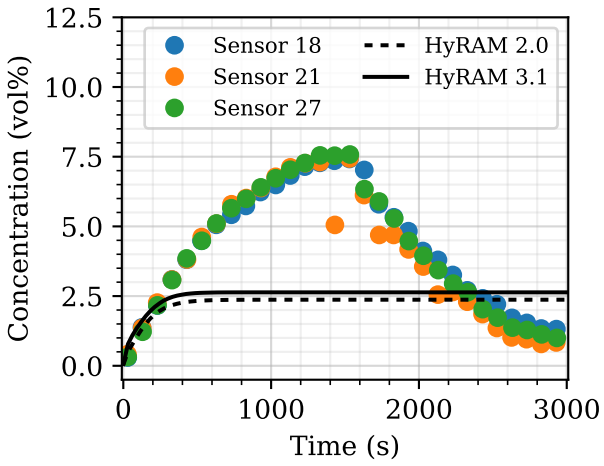

Figure 3-18 Hydrogen concentration measurements along the ceiling from Giannissi et al. [34] compared with HyRAM predictions

In the experiments, all three sensors show an increase in concentration to 7.5% at around 1500 seconds, before starting to reduce. In contrast, HyRAM predicts an increase in concentration to around 2.5%, and remains steady after around 200 seconds into the release. Both HyRAM 2.0 and 3.1 predict this similar steady-state concentrations, which is below the flammability limit for hydrogen of 4%. The experimental data, however, predict peak concentrations of approximately 7.5%. The difference in the predicted vs. measured concentrations is concerning in that it is in non-conservative direction (i.e., HyRAM predicts a lower concentration than measured). This could be because the hydrogen was released vertically and so would have spread a region of higher-concentration mixture as it spread out along the ceiling where the sensors are located. The simplified model in HyRAM, however, assumes that there always exists a perfectly-mixed hydrogen-air mixture along the ceiling. As soon as the release plume enters this layer, it becomes perfectly-mixed as well. Local levels of higher concentration within this layer (such as from plume impingement) are therefore not captured in the simple layer model in HyRAM.

Merilo et al. [35] measured hydrogen releases in a model of a typical residential car garage. The experimental facility had a volume of 60.4 m^3 and both mechanical and natural ventilation openings for different tests. Figure 3-19 shows hydrogen concentration measurements at different heights within the enclosure for different release flowrates and vehicle location tests. The bottom-right frame of Figure 3-19 is for a condition with mechanical ventilation, while the other frames are conditions without mechanical ventilation.

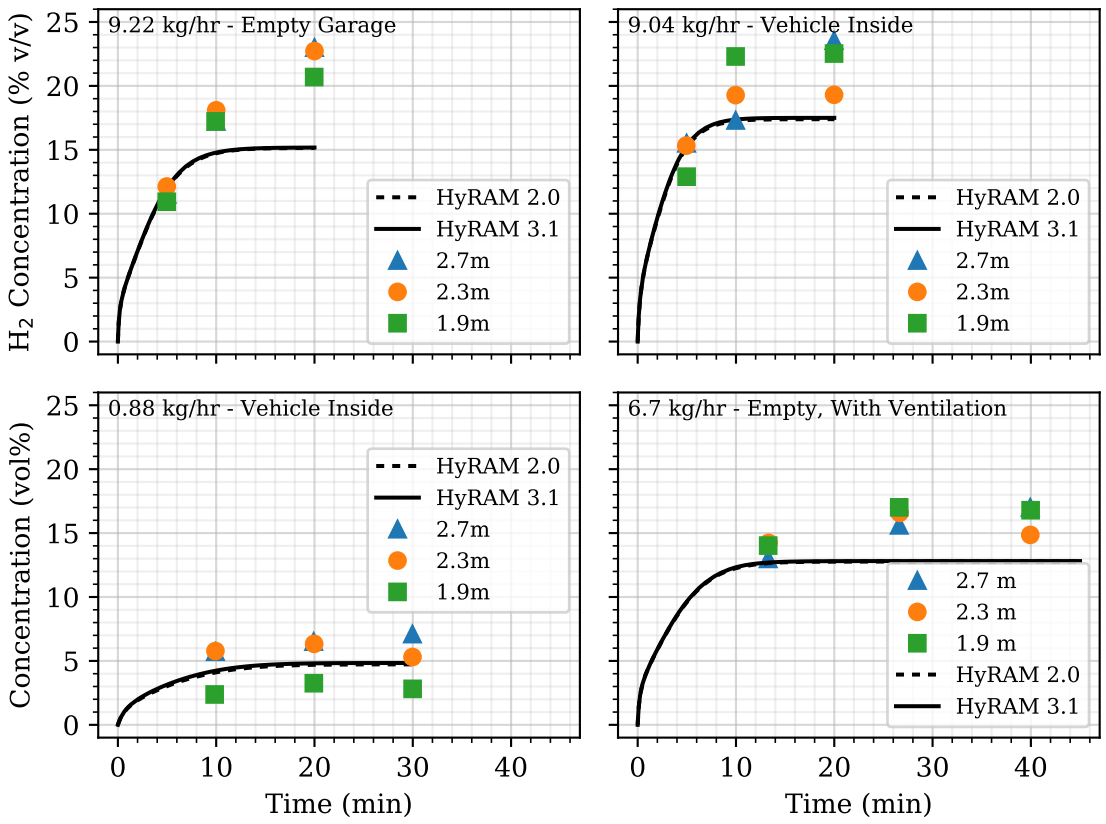

Figure 3-19 Hydrogen concentrations at different heights over time for tests with different hydrogen flowrates and garage open space from Merilo et al. [35] compared to HyRAM predictions. The upper two and lower left frames have only natural ventilation, while the bottom-right frame has 0.1 m^3/s mechanical ventilation.

There is virtually no difference in the predictions between HyRAM 2.0 and 3.1. The rise in concentration predicted by HyRAM is similar to that measured experimentally, although in almost all cases, HyRAM is slightly underpredicting the steady-state concentration. There is no clear correlation in the concentration measured by the sensors at different heights, suggesting that the well-mixed layer model may be acceptable for hydrogen being released into such an enclosure.

Bernard-Michel and Houssin-Agbomson [36] compared releases of helium and hydrogen in enclosures with two ventilation openings. The enclosure was 2 m^3 with a vent at the bottom for inflow and vent at the top for outflow as depicted in Figure 1 of their paper [36]. Hydrogen or helium was released from the bottom of the enclosure vertically, and the injection height varied between 20 cm and 220 cm within the enclosure. Release diameters of 4 mm or 27.2 mm were used and a range of flow rates between 5–240 nL/min were tested. A similar setup was tested for a 1 m^3 enclosure. The concentration of either hydrogen or helium was measured vertically along the enclosure. Figure 3-20a shows the maximum volume concentration of hydrogen for different release flowrates and different orifice sizes at the top of the 2 m^3 enclosure, and Figure 3-20b shows the same data in the 1 m^3 enclosure again measured at the top of the enclosure. Approximately 10 minutes of steady state data was recorded, the specific time of concentration measurements is not provided.

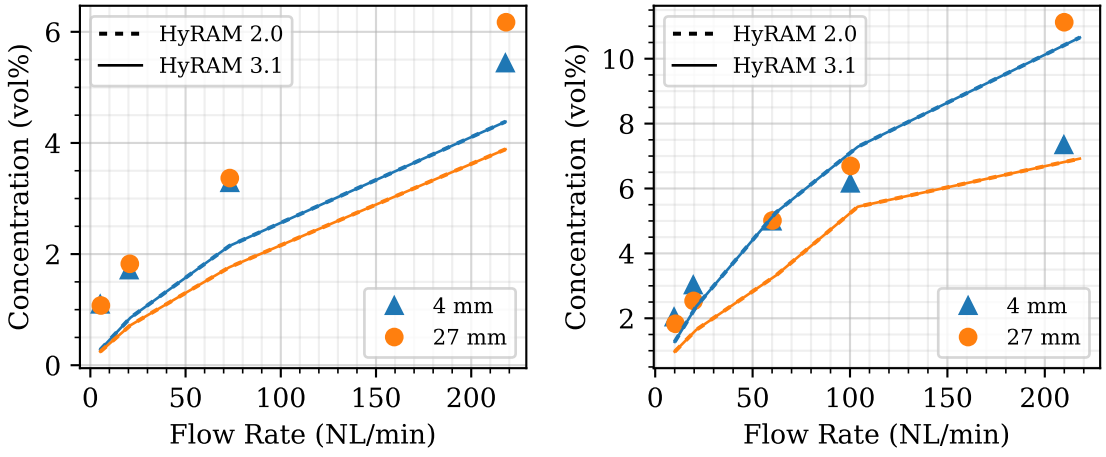

(a) 2 m^3 enclosure

(b) 1 m^3 enclosure

Figure 3-20 Maximum hydrogen concentration values for different release flowrates and orifice sizes in enclosures, with data from Bernard-Michel and Houssin-Agbomson [36] compared to HyRAM

Both versions of HyRAM underpredict the experimental data for the 2 m^3 enclosure (Figure 3-20a) but are much more similar to the data for the 1 m^3 enclosure (Figure 3-20b). The HyRAM models predict higher concentrations for the 4 mm orifice, while the experiments showed higher concentrations for the larger orifice. There is mixing and venting in both the experiments and models, with the models making an assumption of a uniform layer concentration within the top of the enclosure. The physics of this mixing and layering is complex and can be more accurately captured using more complex computational fluid dynamics models. Nonetheless, HyRAM is fairly accurate using the simplifications that enable rapid modeling of these scenarios with low computational overhead.

Overall, HyRAM 3.1 predicts similar accumulation of hydrogen within enclosures to the four sources of experimental data in this section, although some predictions were lower than the measurements. HyRAM 2.0 tends to predict the same or lower concentrations as HyRAM 3.1. HyRAM 3.1 also conservatively predicted the overpressure that would result from the ignition of an accumulated mixture within an enclosure both with and without ventilation while HyRAM 2.0 was non-conservative for the case without ventilation, although there was only a single literature source for this comparison.

3.5. Cryogenic Releases

There are only a handful of groups in the world that have reported on experiments with cryogenic hydrogen. In this section, we compare HyRAM to cryogenic hydrogen dispersion, blowdown, and flame data that is currently available. This includes data from the Karlsruhe Institute of Technology and their partners [37–39], and data from researchers at Sandia National Laboratories [12, 13]. In this section, only HyRAM version 3.1 will be used for comparison, because HyRAM versions ≤ 2.0 are not valid for temperatures $\leq$150 K.

3.5.1. Blowdowns

The Pre-normative Research for Safe use of Liquid Hydrogen (PreSLHy) project funded by the European Fuel Cells and Hydrogen Joint Undertaking (FCH JU) studied several aspects of liquid hydrogen behavior. In one series of experiments, hydrogen at high pressures (5–200 bar) and ambient to low temperatures (80 K) was discharged through a series of orifices. Table 3-6 lists the source of data used as validation for the ignited jet fire model. Several datasets from these experiments are shown in Figures 3-21–3-23.

Table 3-6 Cryogenic Blowdown Validation Data Sources

Author(s)	Year	Figure/Table Number
Friedrich et al. [39]	2019	Directly from dataset

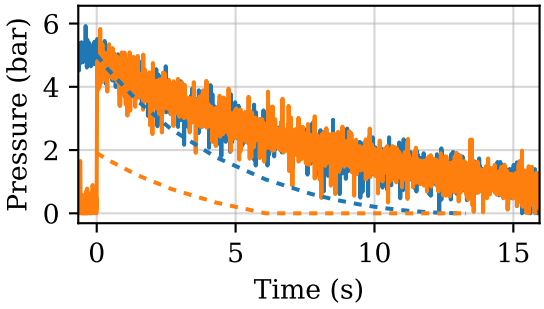

(a) P = 5 bar, T = 80 K, d = 1 mm

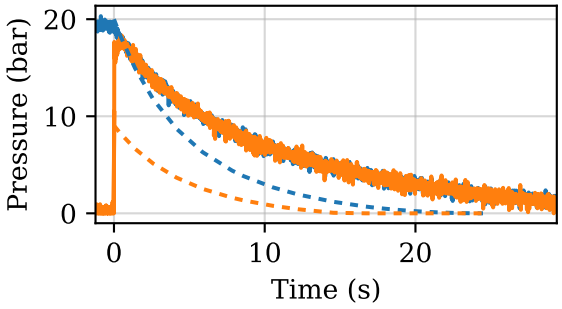

(b) P = 20 bar, T = 80 K, d = 1 mm

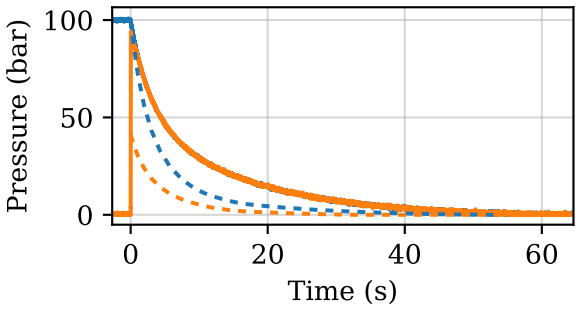

(c) P = 100 bar, T = 80 K, d = 1 mm

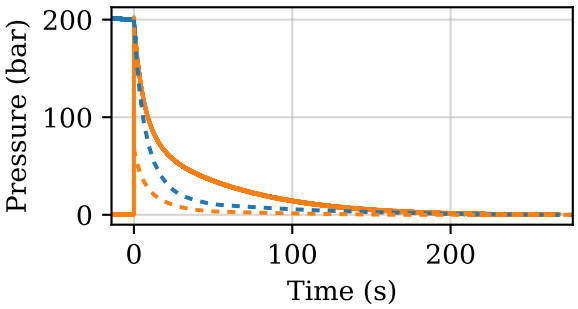

(d) P = 200 bar, T = 80 K, d = 0.5 mm

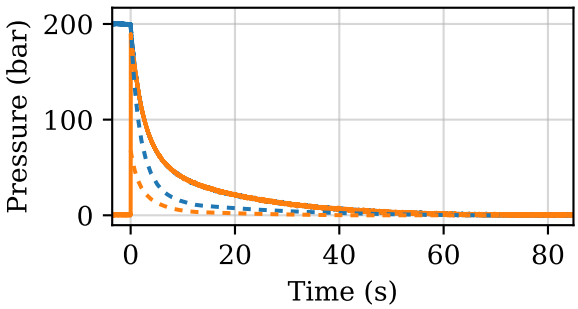

(e) P = 200 bar, T = 80 K, d = 1 mm

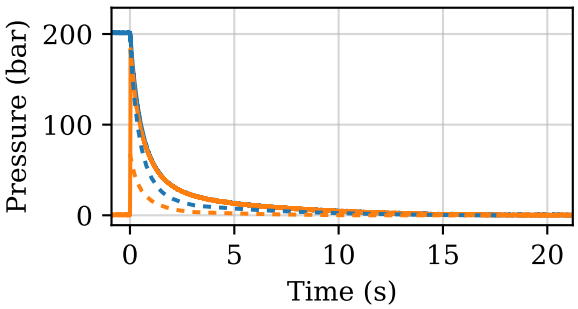

(f) P = 200 bar, T = 80 K, d = 2 mm

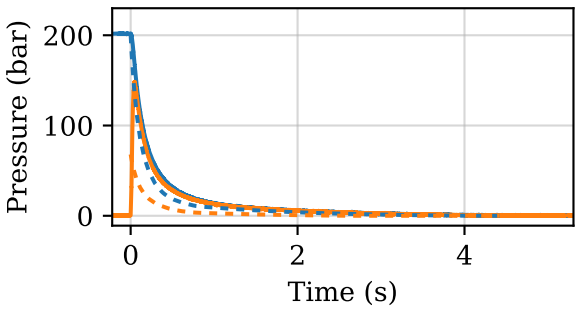

(g) P = 200 bar, T = 80 K, d = 4 mm

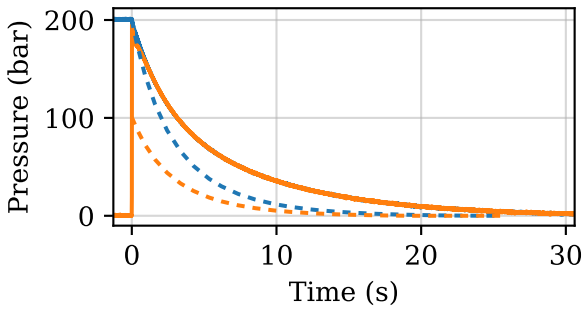

(h) P = 200 bar, T = 300 K, d = 1 mm

Figure 3-21 Pressure during discharge for vessel (blue) and nozzle (orange) for varied pressures, temperatures, and nozzle diameters from Friedrich et al. [39] (solid lines) compared to HyRAM 3.1 (dashed lines)

Figure 3-21 shows the pressure decay both within the vessel and as measured at the nozzle during the discharge experiments. Note that the solid data lines sometimes overlap, making them difficult to distinguish. HyRAM 3.1 (dashed lines) tends to predict a faster pressure decay than was measured experimentally, although the HyRAM prediction for vessel pressure decay better matches for the largest nozzle diameter (Figure 3-21g). Experimentally, there was very little pressure difference observed between the nozzle and vessel pressure, while there is a fairly large pressure difference predicted in HyRAM. The PreSLHy authors [39] do not describe the pressure measurement in detail, and so it is possible that they were measuring the total pressure (which would include a large dynamic pressure due to the high-speed flow) while the HyRAM results are for the static pressure. There are also likely errors in the modeling due to the assumption of isentropic expansion of the fluid into the nozzle while there will be losses in reality. The modeling further assumes a perfectly insulated (adiabatic) tank, but heat flow into the tank also affects the blowdown processes. In all cases, the time to empty (time to reach ambient pressure) is slightly faster for the HyRAM predictions than the experimental data.

Figure 3-22 shows the temperature within the vessel during the discharge. The measurements include three sets of two thermocouples located at the top (blue), center (orange) and bottom (green) of the vessel. In each of the subplots, the temperature measurements for one set of the three thermocouples is 10–20 K lower than the other set of thermocouples. The lower temperature measurements are sheathed thermocouples, while the higher temperatures are unsheathed. The open (unsheathed) thermocouple measurements are marked by a thinner line on the plots, which can be seen by close inspection of Figure 3-22. There are also two measurements of the nozzle temperature. The lower (and thicker) red line is a measurement that is once again a sheathed thermocouple that is mounted in a hole in the nozzle aperture with no direct contact with the flow, while the higher temperature (thin line) is for data from a thermocouple welded into the nozzle line. There are two dashed lines, showing the predicted temperatures by HyRAM – the orange dashed line is the temperature in the vessel (there is only one predicted temperature in the vessel by HyRAM), and the red dashed line is the temperature of the fluid in the nozzle. The sheathed thermocouples agree much better than the open thermocouples with the reported release temperatures at time zero (80 K, or 300 K in Figure 3-22h), and the predicted HyRAM temperatures at time zero in all cases. There appears to be some offset for the unsheathed thermocouples. Also in all cases, the temperature drop within the vessel as the fluid is released is predicted to be much greater than the experimentally measured temperature decrease. This could be due to inaccuracies in the measurements due to the heat capacity of the thermocouples or conduction from the vessel wall along the length of the thermocouples, although they were a small diameter (0.36 mm). Some differences are also likely associated with an adiabatic vessel assumption in HyRAM, while there is heat flow in reality. HyRAM also assumes that the gases in the vessel are instantly and completely well-mixed, while differences in the blue, orange and green traces prove that this is not the case. Similar to the pressure calculations in the nozzle, the temperature predictions in the nozzle are also significantly different (lower) from the temperature in the tank, and lower than the measurements which follow the tank temperature closely (at least the sheathed thermocouple). In addition to measurement errors, the HyRAM model assumes that there is isentropic expansion through the nozzle, while there are losses in reality.

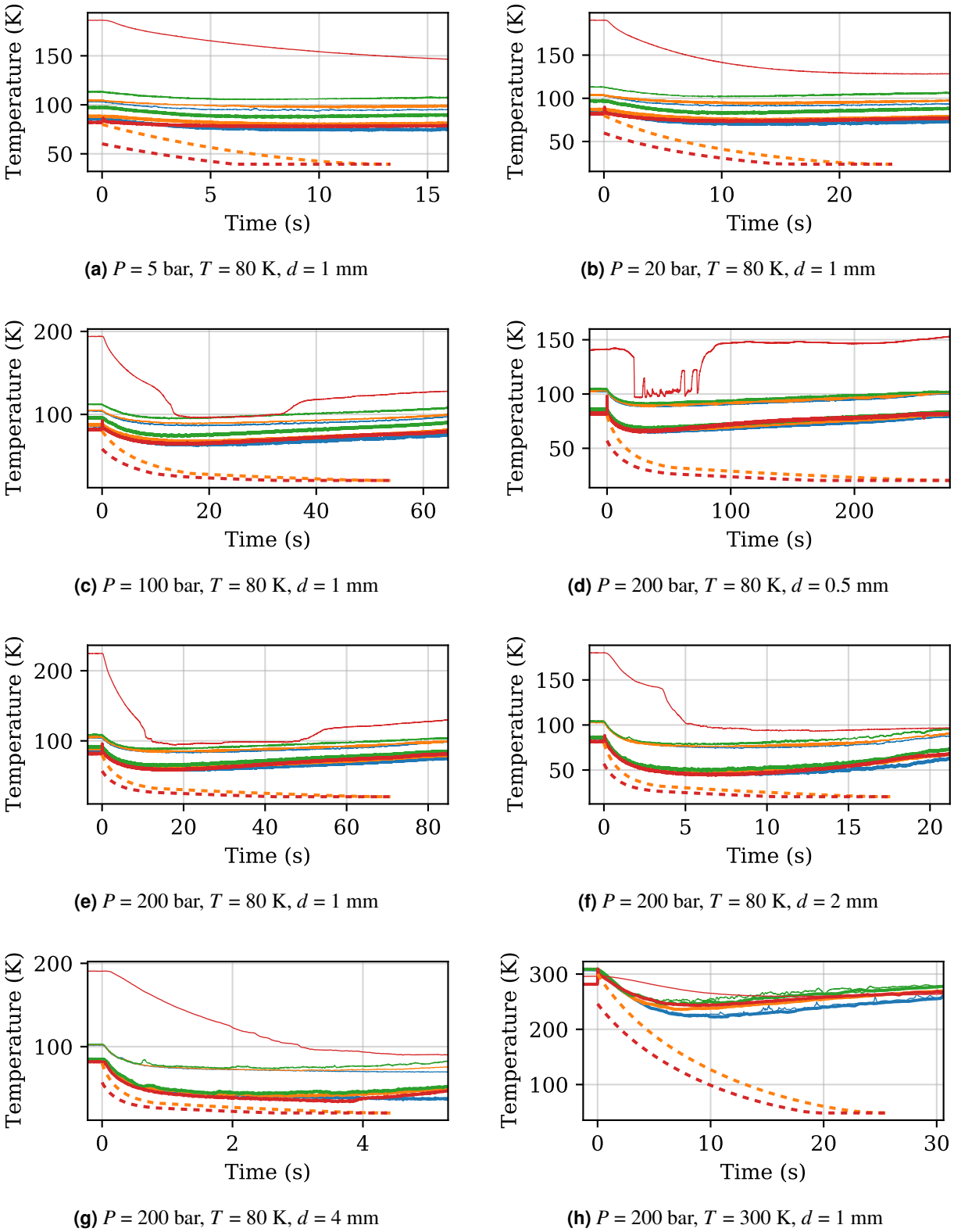

(a) P = 5 bar, T = 80 K, d = 1 mm

(b) P = 20 bar, T = 80 K, d = 1 mm

(c) P = 100 bar, T = 80 K, d = 1 mm

(d) P = 200 bar, T = 80 K, d = 0.5 mm

(e) P = 200 bar, T = 80 K, d = 1 mm

(f) P = 200 bar, T = 80 K, d = 2 mm

(g) P = 200 bar, T = 80 K, d = 4 mm

(h) P = 200 bar, T = 300 K, d = 1 mm

Figure 3-22 Temperature during discharge for vessel top (blue), vessel center (orange), vessel bottom (green), and nozzle (red) as measured by sheathed (thick line) and unsheathed (thin line) thermocouples for varied pressures, temperatures, and nozzle diameters from Friedrich et al. [39] (solid lines) compared to HyRAM 3.1 (dashed lines)

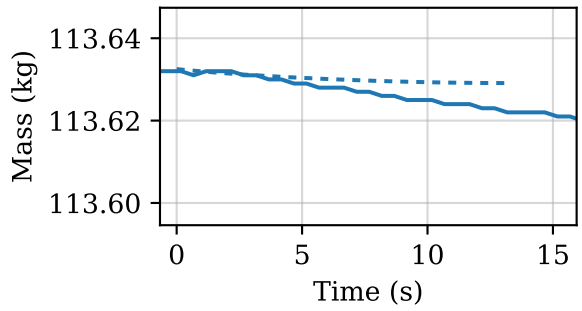

(a) $P = 5$ bar, $T = 80$ K, $d = 1$ mm

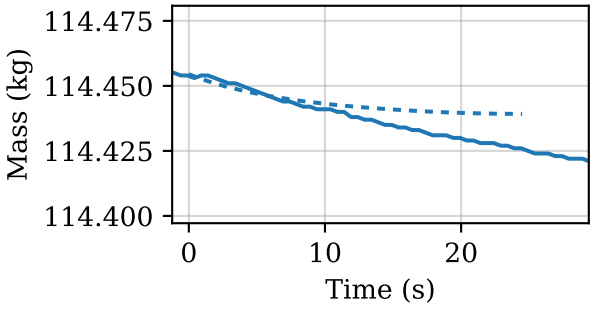

(b) $P = 20$ bar, $T = 80$ K, $d = 1$ mm

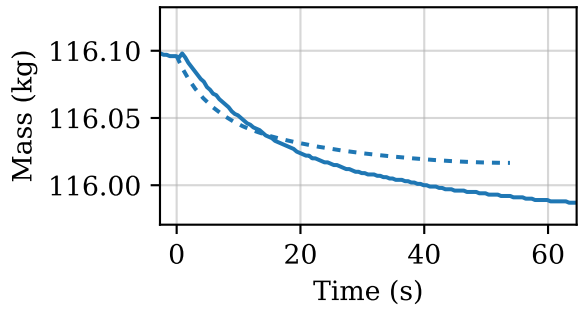

(c) $P = 100$ bar, $T = 80$ K, $d = 1$ mm

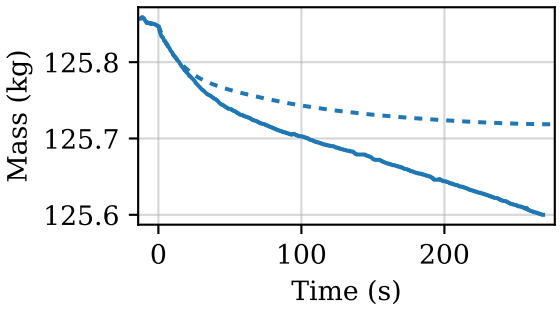

(d) $P = 200$ bar, $T = 80$ K, $d = 0.5$ mm

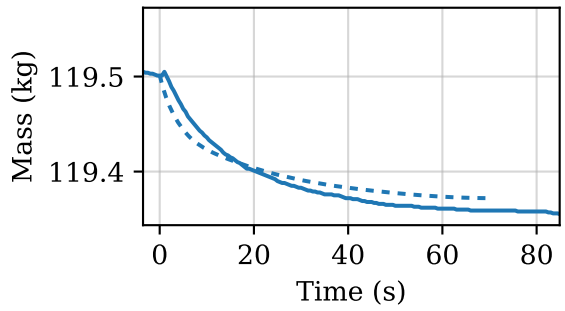

(e) $P = 200$ bar, $T = 80$ K, $d = 1$ mm

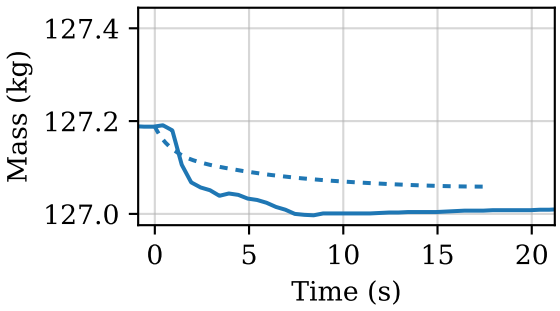

(f) $P = 200$ bar, $T = 80$ K, $d = 2$ mm

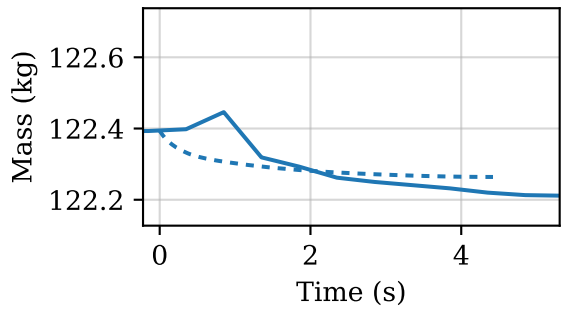

(g) $P = 200$ bar, $T = 80$ K, $d = 4$ mm

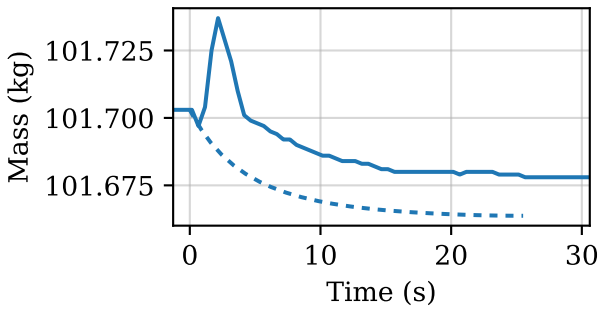

(h) $P = 200$ bar, $T = 300$ K, $d = 1$ mm

Figure 3-23 Tank mass during discharge from Friedrich et al. [39] (solid lines) compared to HyRAM 3.1 (dashed lines)

Figure 3-23 shows the combined mass of both the vessel itself and the hydrogen within the vessel. The HyRAM predictions have the weight of the vessel at time zero added to the mass loss predictions, so that the predictions initially agree with the measurements. The highest mass of hydrogen expelled is a little over 0.1 kg (for 200 bar and 80 K), while the overall weight of the vessel is approximately 120 kg. It is remarkable that the scale is able to capture the small weight loss and not surprising that there are some instances of drift or inaccuracies in the mass measurements. Nonetheless, the HyRAM simulations agree relatively well with the measurements for all diameters, initial pressures, and initial temperatures.

In summary, HyRAM 3.1 predicted slightly faster blowdowns of 80 K hydrogen than were measured in the PreSLHy project [39]. HyRAM accurately predicted the mass loss from the vessel, but lower temperatures within the nozzle and vessel than were measured experimentally.

3.5.2. *Unignited Jet Plumes*

Xiao et al. [37] describe horizontal discharges of room temperature and cryogenic (80 K) hydrogen at pressures from 8.25–68.5 bar. Concentration measurements were taken at several locations downstream of the release point. Table 3-7 lists the tables and figures that were digitized and used as validation for the unignited jet plume model. Figure 3-24 shows the data, along with the calculated inverse mole fraction from HyRAM 3.1.

Table 3-7 Cryogenic Unignited Jet Plumes Validation Data Sources

Author(s)	Year	Figure/Table Number
Xiao et al. [37]	2011	Figure 3
Friedrich et al. [38]	2012	Figure 5
Hecht and Panda [13]	2019	Figure 10, and new data
Friedrich et al. [39]	2019	Directly from dataset

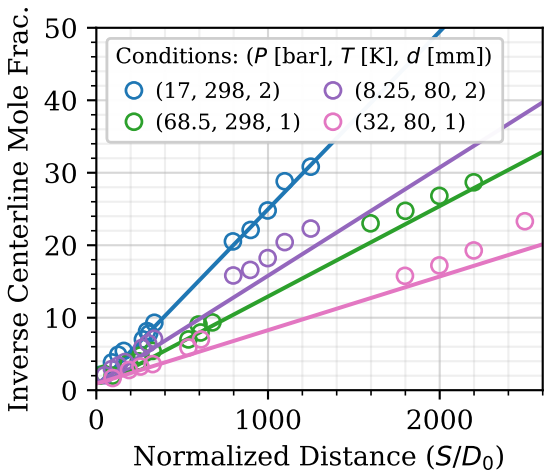

Figure 3-24 Inverse centerline mole fraction as a function of normalized downstream distance for four release scenarios, including two cryogenic (80 K) releases, using data (open circles) from Xiao et al. [37] compared to HyRAM 3.1 (solid lines)

For the range of conditions described by Xiao et al. [37], HyRAM 3.1 results in reasonably accurate predictions of mole fraction as the LFL (inverse mole fraction of 25) is approached and exceeded.

Friedrich et al. [38] describe horizontal discharges of cryogenic (34–65 K) hydrogen at pressures up to 35 bar. Experiments where the hydrogen was ignited are the focus of the paper, but the authors also present some centerline concentration measurements. The normalized jet centerline inverse mole fraction as a function of normalized downstream distance is presented in Figure 3-25.

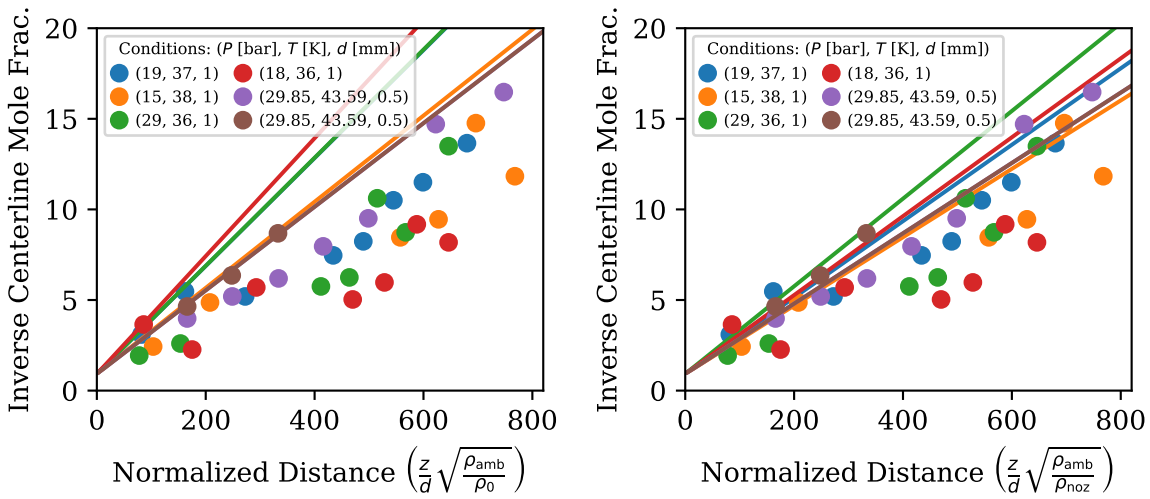

(a) Normalized by stagnation density

(b) Normalized by nozzle density

Figure 3-25 Inverse centerline mole fraction as a function of normalized downstream distance from Friedrich et al. [38] (circles) compared to HyRAM 3.1 (lines)

It can be seen in Figure 3-25a that HyRAM 3.1 underpredicts the mole fractions at large distances (overpredicting the inverse mole fraction), which will result in shorter distances to the LFL than measured experimentally. The authors note in the paper that the concentration decay appears to be slower than for room temperature releases. Since HyRAM 3.1 results agree with room temperature concentration decays (see Section 3.2), this underprediction is not surprising if the authors' observation is true. However, it is possible that the authors incorrectly reported the density used in the normalization of the distance scale. HyRAM results normalized using the nozzle density are shown in Figure 3-25b. If the nozzle density is used rather than the stagnation density, the predictions align more closely with the experimental data.

Hecht and Panda [13] performed lab-scale releases through 1 mm and 1.25 mm nozzles, from 2–5 bar of 45–82 K cryogenic hydrogen. The average mole fraction and temperature fields of these releases were measured using planar laser Raman imaging. The concentration fields are shown in Figure 3-26 and the temperature fields are shown in Figure 3-27. These figures also include some additional data (previously unreported) that was taken after the Hecht and Panda [13] paper was released.

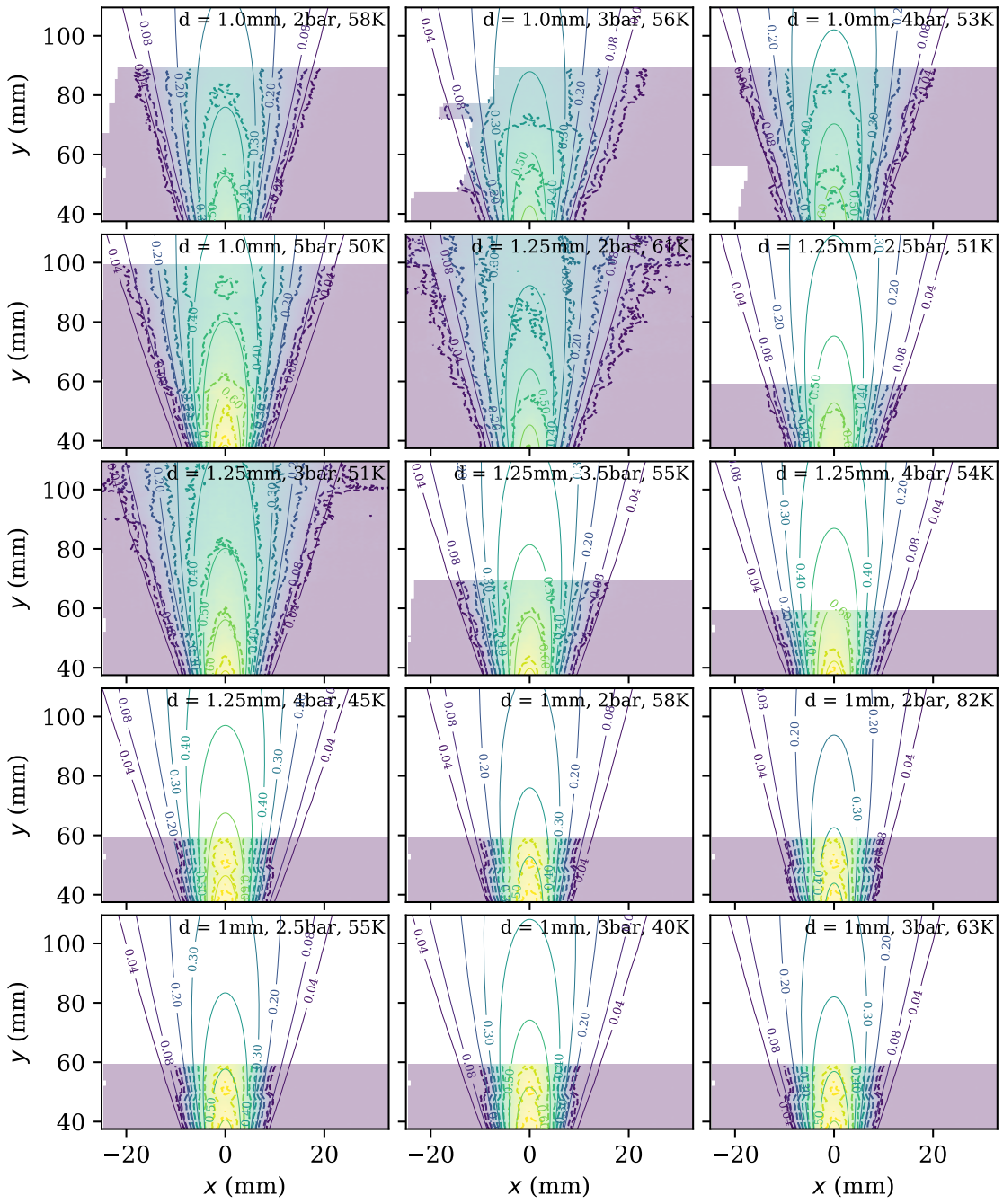

Figure 3-26 Comparison of mole fraction calculated by HyRAM 3.1 (thin, solid lines) to cryogenic hydrogen dispersion data reported by Hecht and Panda [13] (shading and thick, dashed lines) as well as some previously unreported data

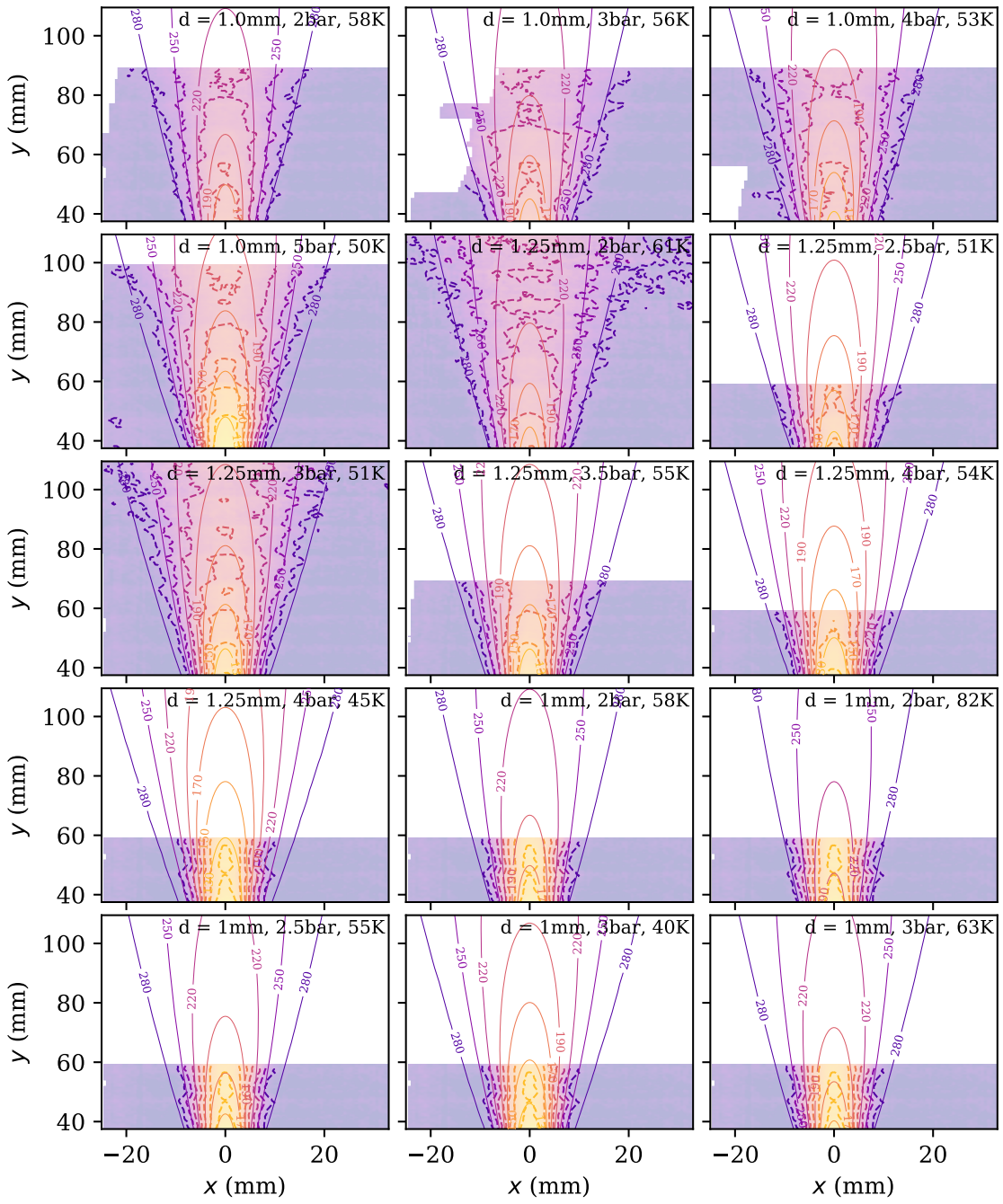

Figure 3-27 Comparison of temperatures calculated by HyRAM 3.1 (thin, solid lines) to cryogenic hydrogen dispersion data reported by Hecht and Panda [13] (shading and thick, dashed lines) as well as some previously unreported data

In these figures, the data is shown by the shading and thick, dashed lines while the HyRAM 3.1 predictions are shown by the thinner, solid lines. While the data is a bit noisy, HyRAM predicts the mole fraction and temperature contours with reasonable accuracy.

The same data from Figures 3-26 and 3-27 are plotted in Figure 3-28. In Figure 3-28, a

two-dimensional histogram with 100 × 100 bins shows a 2D histogram of the difference in predicted mole fraction (Figure 3-28a) or temperature (Figure 3-28b) from HyRAM 3.1 for all of the predicted mole fractions or temperatures.

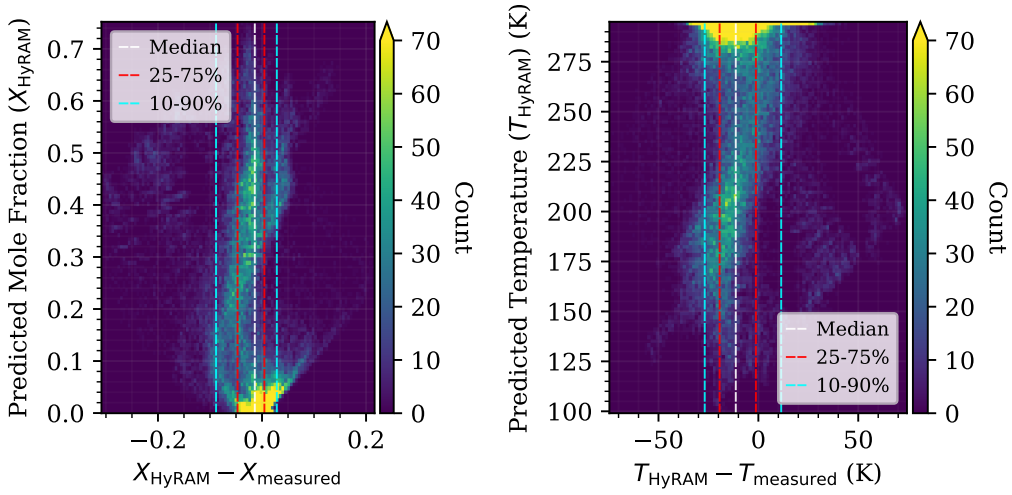

(a) mole fractions **(b)** temperatures

Figure 3-28 Correlation of data to HyRAM for all diameters, pressures, temperatures shown in Figures 3-26 and 3-27 (each point for counting purposes is a 0.5 mm × 0.5 mm pixel)

If all of the data were aligned, it would fall exactly on the 0 point of the *x*-axis. Also shown on the plot are the 1-D median, quartiles, and 10–90% bins of the offset of the data from the predictions (statistic if all of the data for all predicted mole fractions/temperatures were binned). So as not to skew the data, owing to the large fraction of data that is near a hydrogen mole fraction of zero or room temperature, the median, quartiles, and 10–90% bins are only for areas where the simulated mole fraction is above 0.001 (0.1%) or the simulated temperatures are below 293 K. The median predicted mole fraction is 0.014 (1.4%) lower than the measured mole fraction, while the median predicted temperature is 11.3 K lower than the measured temperature. The middle 50% (25–75%) of the predicted mole fractions are within +0.0046/-0.047 of those measured, while 50% of the temperatures are between 1 K and 19 K lower than the measured temperatures. The middle 80% (10–90%) of the simulated mole fractions are within +0.028/-0.088 of the measured mole fractions, and 80% of the simulated temperatures are within +11/-27 K of the measured temperatures. This demonstrates that in general, both mole fraction and temperature predictions are lower than those measured. This could lead to a slightly non-conservative risk prediction for mole fraction (shorter distance to a given concentration), but the magnitude of the error is acceptable, especially given the experimental accuracy.

The discharge experiments described in Section 3.5.1 performed under the Pre-normative Research for Safe use of Liquid Hydrogen (PreSLHy) project [39] also included measurements of concentration and temperature at several locations outside the pressure vessel. A series of pseudo-steady state HyRAM jet simulations were used to calculate predicted mole fractions and temperatures outside the vessel during these blowdowns.

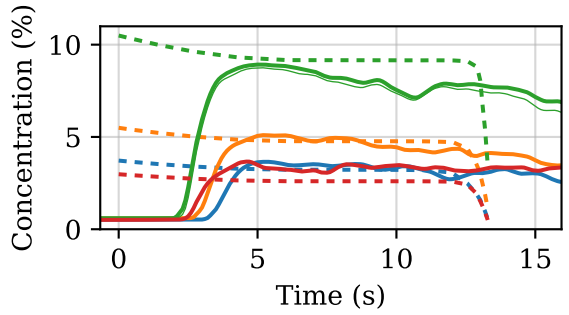

(a) P = 5 bar, T = 80 K, d = 1 mm

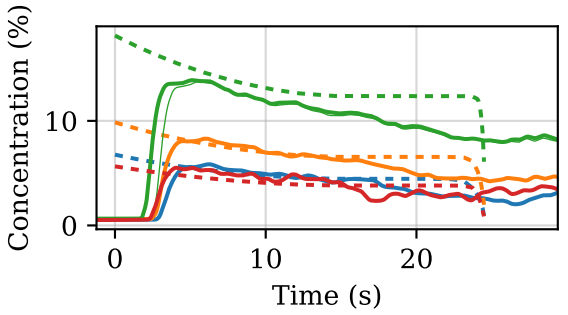

(b) P = 20 bar, T = 80 K, d = 1 mm

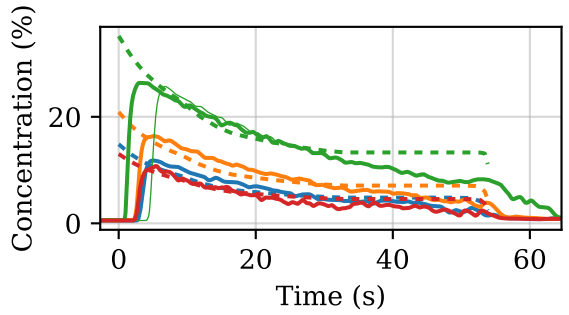

(c) P = 100 bar, T = 80 K, d = 1 mm

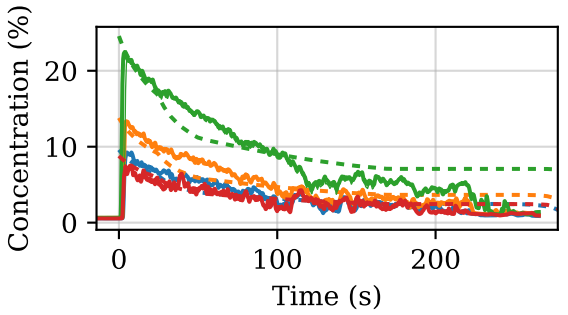

(d) P = 200 bar, T = 80 K, d = 0.5 mm

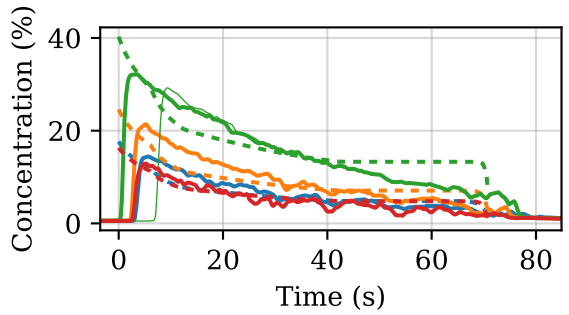

(e) P = 200 bar, T = 80 K, d = 1 mm

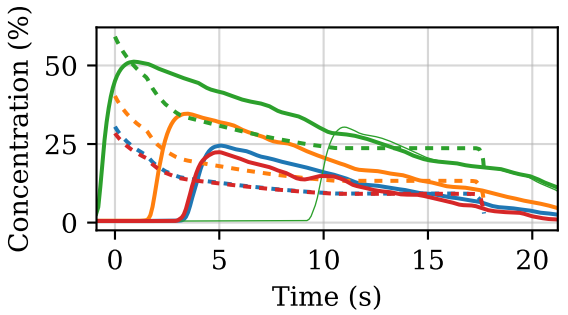

(f) P = 200 bar, T = 80 K, d = 2 mm

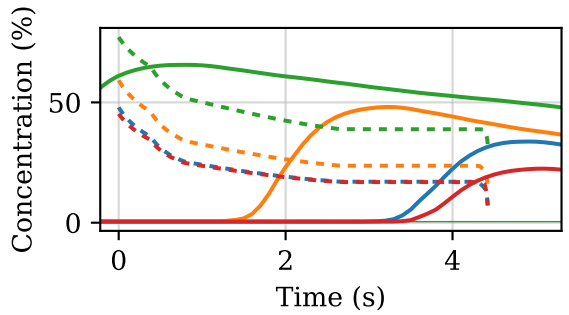

(g) P = 200 bar, T = 80 K, d = 4 mm

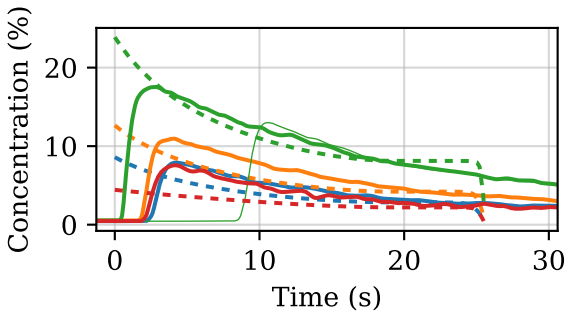

(h) P = 200 bar, T = 300 K, d = 1 mm

Figure 3-29 Molar concentrations during discharge for locations of r = 0 cm, z = 150 cm (blue); r = 0 cm, z = 100 cm (orange); r = 0 cm, z = 50 cm (green - thick and thin lines, with the thin line having a different cut on the extraction probe); and r = 10 cm, z = 100 cm (red) from Friedrich et al. [39] (solid lines) compared to HyRAM 3.1 (dashed lines)

Figure 3-29 shows the molar concentration at several locations outside the vessel during the discharge. The HyRAM simulations to which these measurements are compared (dashed lines) are a series of pseudo-steady-state simulations using the tank conditions predicted at multiple times during the blowdowns (i.e., steady-state jet models of the conditions shown by the dashed lines in Figures 3-21 and 3-22). In all cases (including the 300 K release, Figure 3-29h), the concentrations initially peak and then decays back towards zero. There is clearly a time lag in the concentration measurements, as the measured concentrations do not increase exactly at time zero (this is especially evident in Figure 3-29g where the flow time is short). However, generally the mole concentration measurements agree reasonably well with the model, regardless of the orifice diameter, initial pressure, or initial temperature. Figures 3-29f and 3-29g have the poorest agreement with the model, likely due to the short blowdown time and the time lag, low speed data collection, and averaging by the concentration sensors due to transport through the extraction lines and sensor response time.

Figure 3-30 shows the temperature at several locations outside the vessel during the discharge. Similar to the concentrations (Figure 3-29), the HyRAM simulations to which these measurements are compared (dashed lines) are a series of pseudo-steady-state simulations using the tank conditions predicted at multiple times during the blowdowns. Analgous to the concentration data (Figure 3-29), the temperatures initially drop and then rises back towards ambient, even for the ambient temperature release (Figure 3-30h). The temperatures outside of the vessel measured by the experiment are generally higher than those predicted by HyRAM. However, as the orifice diameter becomes large (e.g., Figure 3-30g), the level of agreement with the experimentally measured temperatures improves. This may indicate that the thermal mass/heat capacity of the thermocouples is important, such that the measured temperatures are not indicative of the actual gas temperature for the lower flows (smaller diameters, lower pressures, or higher initial temperatures). This is because there is may not be enough flow to lower the temperature of the thermocouples. The disagreement in measured and predicted temperatures could also arise from the HyRAM model assumptions of isentropic of flow through the nozzle and an adiabatic tank, as the temperatures in the vessel and nozzle were also predicted to be lower than those measured experimentally (Figure 3-22). This is especially obvious for the orange and blue data lines, which show some of the largest differences between data and predictions. This is likely due to the sensor locations that are the closest to the release point (r = 0 cm, z = 25 cm and r = 2 cm, z = 20 cm), meaning that the HyRAM model assumptions that predict lower gas temperatures would be the most pronounced for this case.

In general, HyRAM accurately predicted the concentrations and concentration decay for unignited jet plumes from cryogenic releases, but predicted lower temperatures than were measured experimentally.

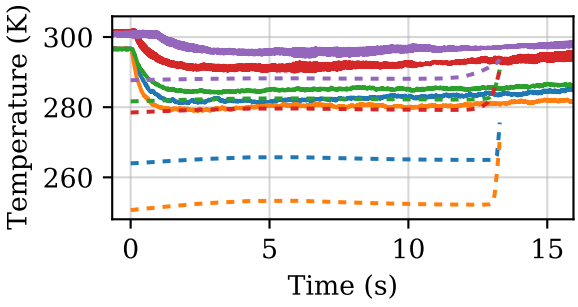

(a) P = 5 bar, T = 80 K, d = 1 mm

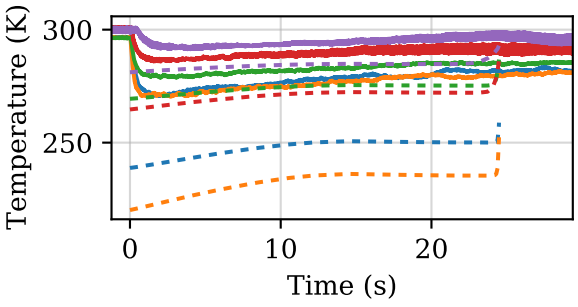

(b) P = 20 bar, T = 80 K, d = 1 mm

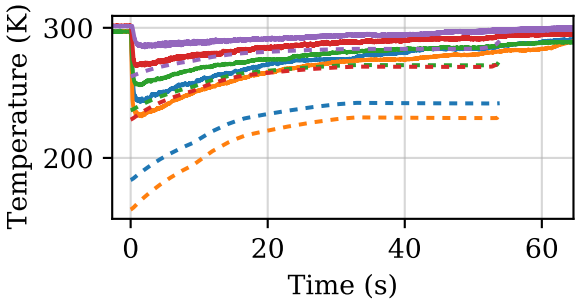

(c) P = 100 bar, T = 80 K, d = 1 mm

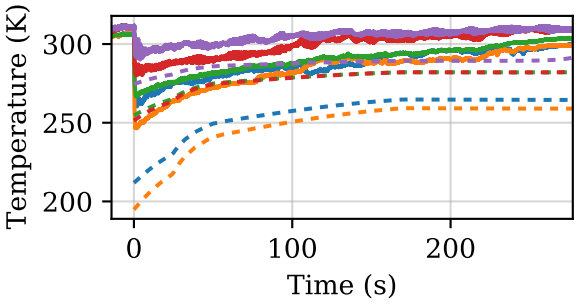

(d) P = 200 bar, T = 80 K, d = 0.5 mm

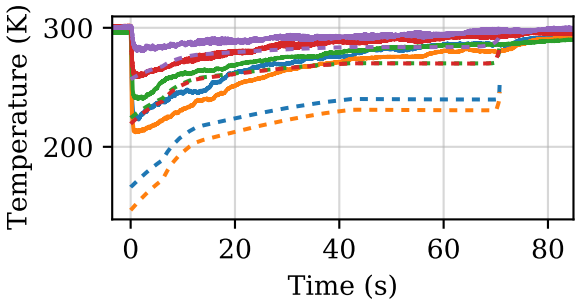

(e) P = 200 bar, T = 80 K, d = 1 mm

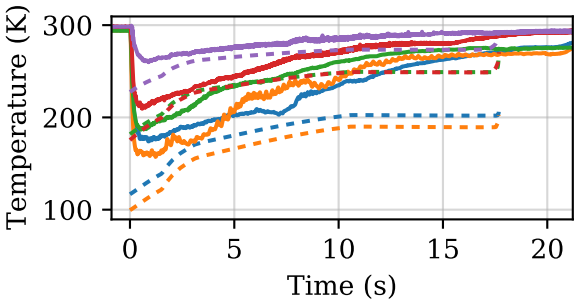

(f) P = 200 bar, T = 80 K, d = 2 mm

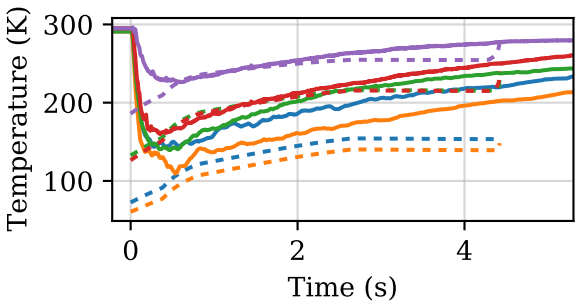

(g) P = 200 bar, T = 80 K, d = 4 mm

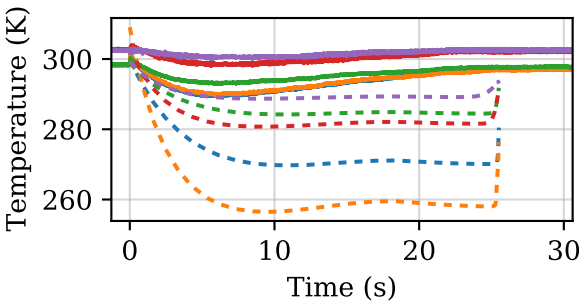

(h) P = 200 bar, T = 300 K, d = 1 mm

Figure 3-30 Temperatures outside the vessel during discharge for locations of r = 2 cm, z = 20 cm (blue); r = 0 cm, z = 25 cm (orange); r = 5 cm, z = 50 cm (green); r = 0 cm, z = 75 cm (red); and r = 0 cm, z = 175 cm (purple) from Friedrich et al. [39] (solid lines) compared to HyRAM 3.1 (dashed lines)

3.5.3. Ignited Jet Fires

Panda and Hecht [12] measured lab scale flames of hydrogen with release temperatures from 46–295 K, through nozzles from 0.75–1.25 mm, at pressures from 1–5 bar_g. Table 3-8 lists the tables and figures that were digitized and used as validation for the blowdown model. The HyRAM predicted flame lengths are shown relative to the measured flame lengths in Figure 3-31.

Table 3-8 Cryogenic Ignited Jet Plumes Validation Data Sources

Author(s)	Year	Figure/Table Number
Panda and Hecht [12]	2017	Table 3

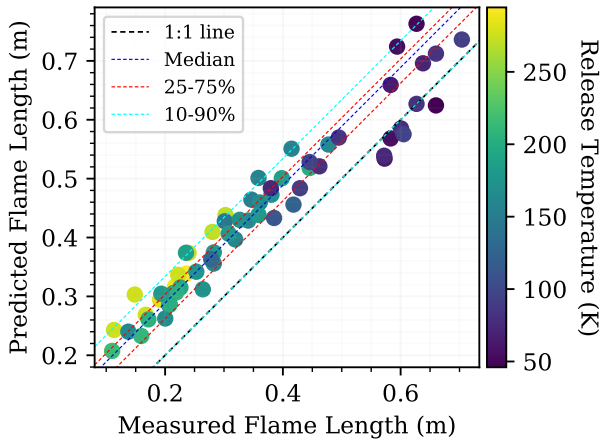

Figure 3-31 Comparison of flame length calculated by HyRAM 3.1 to those measured by Panda and Hecht [12]

Similar to Figures 3-26 and 3-27, the median, middle 50% and middle 80% of the data are also shown in Figure 3-31. In this case, the predicted flame lengths are mostly above the measured flame lengths, with the median flame length 9 cm longer than the measured flame length, the middle 50% of the conditions having flames 6–10 cm longer than those measured, and 80% of the data between 0–13 cm longer than the measured flame length. These longer predicted flame lengths will result in conservative predictions of risk.

Panda and Hecht [12] also measured the radiant heat flux from cryogenic hydrogen flames, with the conditions listed previously (temperatures from 46–295 K, through nozzles from 0.75–1.25 mm, at pressures from 1–5 bar_g). Calculated heat fluxes for each of the radiometers used in the experiments are shown as a function of the measured heat flux in Figure 3-32.

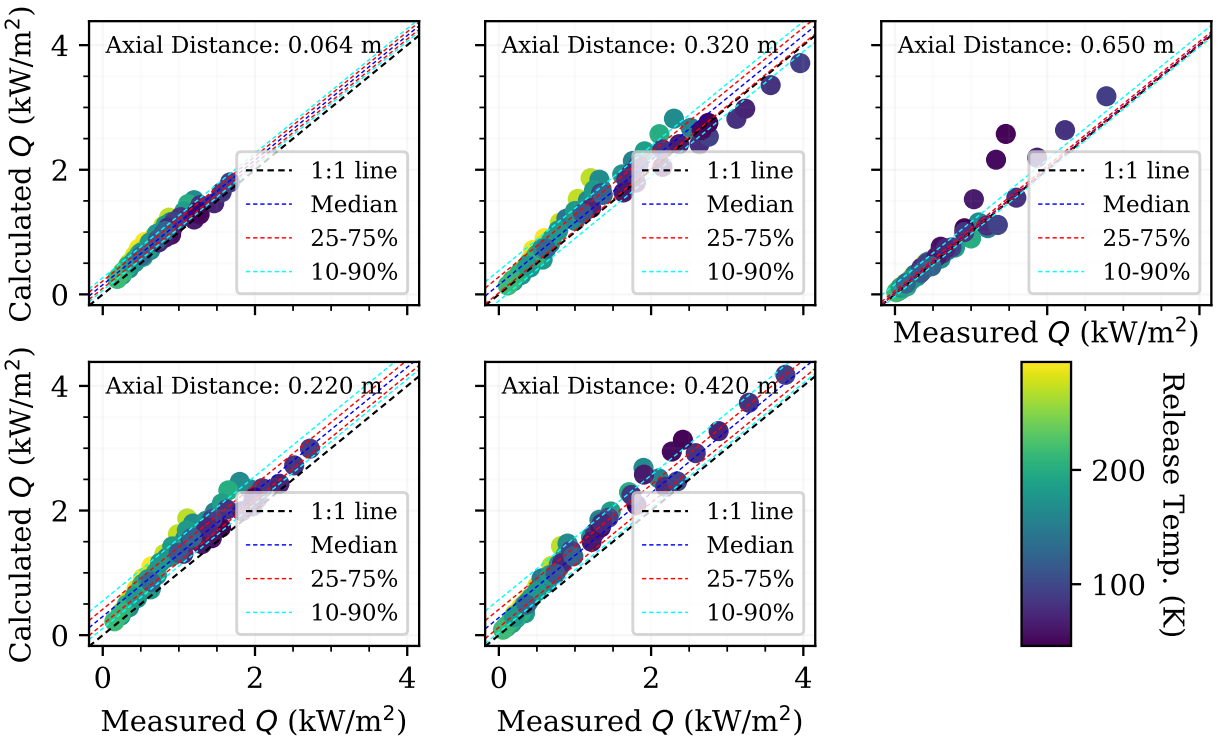

Figure 3-32 Comparison of heat flux (Q) calculated by HyRAM 3.1 to those measured by Panda and Hecht [12]

The median calculated heat fluxes for all locations are larger than the predicted heat fluxes, as is the majority of the data. For each of the radiometers, the middle 50% of the calculated heat fluxes are larger than those measured, and only at axial distances of 0.32 m and 0.65 m are more than 10% of the calculated heat fluxes lower than the measured heat fluxes (the lowest teal lines are slightly below the 1:1 lines). Similar to the flame lengths, a larger calculated heat flux will result in a conservative analysis as to the safety of a cryogenic hydrogen flame.

This page intentionally left blank.

4. CONCLUSIONS

HyRAM 3$\geq$ 3.0 contains some significant changes compared to HyRAM 2.0 and earlier. One primary change is the use of a real gas equation of state rather than the Abel-Noble equation of state that is used in version 2.0 or less. This change enables the use of HyRAM 3 for cryogenic hydrogen flows whereas the Abel-Noble equation of state is not accurate at low temperatures. In addition to the real gas equation of state, several more minor updates the physics models were made (see Section 1.2.2). In this report, we have compared HyRAM 3.1 results to experimental data from the literature in order to demonstrate the accuracy of the physics models. HyRAM 3.1 results were also compared to HyRAM 2.0 for high-pressure, non-cryogenic flows to highlight the differences in predictions between the two major versions of HyRAM.

The blowdown (emptying) of high-pressure, room-temperature tanks predicted by HyRAM 3.1 and 2.0 are compared to four literature sources in Section 3.1. Data was gathered for hydrogen tanks with initial pressures of 13.45 MPa, 15.5 MPa, 43.1 MPa, and 90 MPa. HyRAM 2.0 and 3.1 predict very similar pressure losses and flow rates during the course of the blowdowns, and the times to empty were very similar to the experiments. The tank temperature was also monitored in one experiment and in this case, both versions of HyRAM predicted much lower tank temperatures than the experimental measurements. This is likely due to gas mixing within the tank and heat flow through the tank walls, which are not accounted for in either version of HyRAM.

Mean concentrations (mole and mass fractions) during the dispersion of hydrogen are compared for a range of release scenarios in Section 3.2. HyRAM 3.1 predicts a faster centerline concentration decay than HyRAM 2.0 in most scenarios. This difference is primarily due to increased momentum driven entrainment in HyRAM 3.1 over HyRAM 2.0. HyRAM 3.1 uses the properties of the fluid at the notional nozzle to calculate momentum driven entrainment while HyRAM 2.0 uses the properties at the actual nozzle/orifice. Increased momentum driven entrainment and a faster centerline concentration decay reduces the dilution length (distance to a given concentration). Dilution length is generally used to specify distances in risk analyses, meaning that HyRAM 3.1 is less conservative than HyRAM 2.0 in this context. HyRAM 2.0 tends to predict mean centerline mole fractions that are greater than the literature data while HyRAM 3.1 generally provides better agreement along the centerline. Neither version 2.0 nor 3.1 of HyRAM is particularly accurate at predicting the width of the Gaussian dispersion profile. Improved tuning of empirical parameter values within the HyRAM model may improve this agreement, but this needs to be explored further.

Flame lengths and heat fluxes for ignited high-pressure hydrogen diffusion flames are predicted and compared to a variety of literature data in Section 3.3. Updates to HyRAM 3.1 from 2.0 minimally affects prediction of flame length or heat flux, with HyRAM 3.1 producing minimally more conservative values (a longer flame length and higher heat flux). Overall, both versions of HyRAM accurately predict both flame length and heat flux, for hydrogen diffusion flames up to 900 bar.

Accumulation within an enclosure and the overpressure that would result if the accumulated hydrogen were to ignite are compared to several literature sources in Section 3.4. HyRAM 3.1

predicts similar or higher concentrations within an enclosure than HyRAM 2.0. In one case, HyRAM 2.0 predicted a lower peak overpressure than was measured experimentally, for an enclosure without ventilation while HyRAM 3.1 predicted a higher peak overpressure than the measurement (i.e., HyRAM 3.1 provided a conservative result). Both versions of HyRAM 2.0 and 3.1 predict concentrations and overpressures that are similar to literature data, but there is a fairly wide variability in accuracy, depending on the exact experimental setup.

Finally, HyRAM 3.1 is compared to literature data for cryogenic releases of hydrogen in Section 3.5. Only HyRAM 3.1 is compared to cryogenic releases due to the inapplicability of HyRAM 2.0 at the low temperatures. Similar to the room-temperature blowdown simulations, HyRAM 3.1 fairly accurately predicts the pressure decay as a tank is emptied, but predicts temperatures in the tank that are much lower than the measured experimental data. HyRAM 3.1 also predicts significant differences in the pressure and temperature in the orifice vs. the tank, while the pressure and temperature measured at the orifice and tank in the experiments were similar. HyRAM 3.1 predicts centerline concentration decay and even two-dimensional near-field concentration fields of unignited jets accurately. HyRAM 3.1 tends to slightly overpredict concentration in most cases, while some temperature measurements were higher and some lower than those predicted. In most of the experiments, the temperature measurements had more uncertainty than the concentration measurements. Similar to the warm releases, HyRAM 3.1 also predicts slightly longer visible flame lengths and heat fluxes than were measured experimentally.

Overall, HyRAM 3.1 improves on the accuracy of the physical models relative to HyRAM 2.0. This reduces the conservatism in risk calculations using HyRAM. Both versions 2.0 and 3.1 of HyRAM are accurate for predictions of blowdowns, diffusion jets, and diffusion flames of hydrogen at pressures up to 900 bar, and HyRAM 3.1 also shows good agreement with cryogenic hydrogen data. Improvements could be made to the two-dimensional (width) of the dispersion predictions as well as the indoor accumulation and overpressure models. As additional data for cryogenic hydrogen behavior becomes available, additional comparisons and model improvements should be made.

REFERENCES

[1] K. M. Groth, E. S. Hecht, and J. T. Reynolds, "Methodology for assessing the safety of Hydrogen Systems: HyRAM 1.0 technical reference manual," Sandia National Laboratories, SAND2015-10216, November 2015.

[2] K. M. Groth, E. S. Hecht, J. T. Reynolds, M. L. Blaylock, and E. E. Carrier, "Methodology for assessing the safety of Hydrogen Systems: HyRAM 1.1 technical reference manual," Sandia National Laboratories, SAND2017-2998, March 2017.

[3] G. Feliciano Morales, B. D. Ehrhart, and A. B. Muna, "HyRAM V2.0 User Guide," Sandia National Laboratories, SAND2019-8940, July 2019.

[4] B. D. Ehrhart and E. S. Hecht, "Hydrogen Risk Assessment Models (HyRAM) Version 3.0 Technical Reference Manual," Sandia National Laboratories, SAND2020-10600, September 2020.

[5] ——, "Hydrogen Risk Assessment Models (HyRAM) Version 3.1 Technical Reference Manual," Sandia National Laboratories, SAND2021-5812, May 2021.

[6] W. Houf and R. Schefer, "Analytical and experimental investigation of small-scale unintended releases of hydrogen," *International Journal of Hydrogen Energy*, vol. 33, no. 4, pp. 1435–1444, February 2008.

[7] W. S. Winters, "Modeling Leaks from Liquid Hydrogen Storage Systems," Sandia National Laboratories, SAND2009-0035, January 2009.

[8] W. Houf and W. Winters, "Simulation of high-pressure liquid hydrogen releases," *International Journal of Hydrogen Energy*, vol. 38, no. 19, pp. 8092–8099, June 2013.

[9] W. Houf and R. Schefer, "Predicting radiative heat fluxes and flammability envelopes from unintended releases of hydrogen," *International Journal of Hydrogen Energy*, vol. 32, no. 1, pp. 136–151, January 2007.

[10] I. Ekoto, A. Ruggles, L. Creitz, and J. Li, "Updated jet flame radiation modeling with buoyancy corrections," *International Journal of Hydrogen Energy*, vol. 39, no. 35, pp. 20 570–20 577, December 2014.

[11] G. Hankinson and B. J. Lowesmith, "A consideration of methods of determining the radiative characteristics of jet fires," *Combustion and Flame*, vol. 159, no. 3, pp. 1165–1177, March 2012.

[12] P. P. Panda and E. S. Hecht, "Ignition and flame characteristics of cryogenic hydrogen releases," *International Journal of Hydrogen Energy*, vol. 42, no. 1, pp. 775–785, January 2017.

[13] E. S. Hecht and P. P. Panda, "Mixing and warming of cryogenic hydrogen releases," *International Journal of Hydrogen Energy*, vol. 44, no. 17, pp. 8960–8970, April 2019.

[14] E. S. Hecht, P. P. Panda, B. R. Chowdhury, and D. Ye, "Characteristics of cryogenic hydrogen releases under unignited and ignited conditions," Sandia National Laboratories, SAND2019-9998, August 2019.

[15] J. W. Leachman, R. T. Jacobsen, S. G. Penoncello, and E. W. Lemmon, "Fundamental equations of state for parahydrogen, normal hydrogen, and orthohydrogen," *Journal of Physical and Chemical Reference Data*, vol. 38, no. 3, pp. 721–748, 2009.

[16] I. H. Bell, J. Wronski, S. Quoilin, and V. Lemort, "Pure and pseudo-pure fluid thermophysical property evaluation and the open-source thermophysical property library coolprop," *Industrial & Engineering Chemistry Research*, vol. 53, no. 6, pp. 2498–2508, January 2014.

[17] X. Li, E. S. Hecht, and D. M. Christopher, "Validation of a reduced-order jet model for subsonic and underexpanded hydrogen jets," *International Journal of Hydrogen Energy*, vol. 41, no. 2, pp. 1348–1358, January 2016.

[18] A. Rohatgi, *WebPlotDigitizer*, July, 2020. [Online]. Available: https://automeris.io/WebPlotDigitizer

[19] I. W. Ekoto, W. G. Houf, G. H. Evans, E. G. Merilo, and M. A. Groethe, "Experimental investigation of hydrogen release and ignition from fuel cell powered forklifts in enclosed spaces," *International Journal of Hydrogen Energy*, vol. 37, no. 22, pp. 17 446–17 456, November 2012.

[20] R. Schefer, W. Houf, T. Williams, B. Bourne, and J. Colton, "Characterization of high-pressure, underexpanded hydrogen-jet flames," *International Journal of Hydrogen Energy*, vol. 32, no. 12, pp. 2081–2093, August 2007.

[21] C. Proust, D. Jamois, and E. Studer, "High pressure hydrogen fires," *International Journal of Hydrogen Energy*, vol. 36, no. 3, pp. 2367–2373, February 2011.

[22] R. Schefer, W. Houf, B. Bourne, and J. Colton, "Spatial and radiative properties of an open-flame hydrogen plume," *International Journal of Hydrogen Energy*, vol. 31, no. 10, pp. 1332–1340, August 2006.

[23] V. Molkov, *Fundamentals of Hydrogen Safety Engineering I*. bookboon.com, 2012.

[24] A. Ruggles and I. Ekoto, "Ignitability and mixing of underexpanded hydrogen jets," *International Journal of Hydrogen Energy*, vol. 37, no. 22, pp. 17 549–17 560, November 2012.

[25] S. H. Han, D. Chang, and J. S. Kim, "Release characteristics of highly pressurized hydrogen through a small hole," *International Journal of Hydrogen Energy*, vol. 38, no. 8, pp. 3503–3512, March 2013.

[26] J. Chaineaux, G. Mavrothalassitis, and J. Pineau, "Modelization and validation of the discharge in air of a vessel pressurized by flammable gas," *Progress in Astronautics and Aeronautics*, vol. 134, pp. 104–137, 1991.

[27] M. Kuznetsov, "Hydrogen distribution tests in free turbulent jet," FZK, SBEP V4, 2006.

[28] K. Okabayashi, T. Nonaka, N. Sakata, K. Takeno, H. Hirashima, and K. Chitose, "Characteristics of dispersion for leakage of high-pressurized hydrogen gas," *Japan Society for Safety Engineering*, vol. 44, pp. 391–397, 2005.

[29] E. Ruffin, Y. Mouilleau, and J. Chaineaux, "Large scale characterization of the concentration field of supercritical jets of hydrogen and methane," *Journal of Loss Prevention in the Process Industries*, vol. 9, no. 4, pp. 279–284, 1996.

[30] L. Shirvill, P. Roberts, T. Roberts, C. Butler, and M. Royle, "Dispersion of hydrogen from high-pressure sources," in *Proceedings of the IChemE Symposium Hazards XIX*, March 2006.

[31] A. Veser, M. Kuznetsov, G. Fast, A. Friedrich, N. Kotchourko, G. Stern, M. Schwall, and W. Breitung, "The structure and flame propagation regimes in turbulent hydrogen jets," in *Proceedings of the Third International Conference on Hydrogen Safety*, September 2009.

[32] T. Imamura, S. Hamada, T. Mogi, Y. Wada, S. Horiguchi, A. Miyake, and T. Ogawa, "Experimental investigation on the thermal properties of hydrogen jet flame and hot currents in the downstream region," *International Journal of Hydrogen Energy*, vol. 33, no. 13, pp. 3426–3435, July 2008.

[33] T. Mogi, H. Nishida, and S. Horiguchi, "Flame characteristics of high-pressure hydrogen gas jet," in *Proceedings of the first International Conference on Hydrogen Safety (ICHS 2005)*, September 2005.

[34] S. Giannissi, J. Hoyes, B. Chernyavskiy, P. Hooker, J. Hall, A. Venetsanos, and V. Molkov, "CFD benchmark on hydrogen release and dispersion in a ventilated enclosure: Passive ventilation and the role of an external wind," *International Journal of Hydrogen Energy*, vol. 40, no. 19, pp. 6465–6477, May 2015.

[35] E. Merilo, M. Groethe, J. Colton, and S. Chiba, "Experimental study of hydrogen release accidents in a vehicle garage," *International Journal of Hydrogen Energy*, vol. 36, no. 3, pp. 2436–2444, February 2011.

[36] G. Bernard-Michel and D. Houssin-Agbomson, "Comparison of helium and hydrogen releases in 1 m^3 and 2 m^3 two vents enclosures: Concentration measurements at different flow rates and for two diameters of injection nozzle," *International Journal of Hydrogen Energy*, vol. 42, no. 11, pp. 7542–7550, March 2017.

[37] J. Xiao, J. Travis, and W. Breitung, "Hydrogen release from a high pressure gaseous hydrogen reservoir in case of a small leak," *International Journal of Hydrogen Energy*, vol. 36, no. 3, pp. 2545–2554, February 2011.

[38] A. Friedrich, W. Breitung, G. Stern, A. Veser, M. Kuznetsov, G. Fast, B. Oechsler, N. Kotchourko, T. Jordan, J. Travis, J. Xiao, M. Schwall, and M. Rottenecker, "Ignition and heat radiation of cryogenic hydrogen jets," *International Journal of Hydrogen Energy*, vol. 37, no. 22, pp. 17 589–17 598, November 2012.

[39] A. Friedrich, A. Vesser, and T. Jordan. PRESLHY experiment series E3.1 (cryogenic hydrogen blow-down/discharge) results. [Online]. Available: http://dx.doi.org/10.5445/IR/1000096833

[40] R. Schefer, W. Houf, and T. Williams, "Investigation of small-scale unintended releases of hydrogen: momentum-dominated regime," *International Journal of Hydrogen Energy*, vol. 33, no. 21, pp. 6373–6384, 2008.

APPENDIX A. VALIDATION DATA INPUT PARAMETERS

This section contains a summary of all inputs used in HyRAM models for comparison to experimental data. For each set of inputs, the value and unit for each parameter is given, along with the location within the cited source from which the input was obtained.

A.1. Blowdown Input Parameters

Table A-1 Ekoto et al. [19] Figure 3 Input Parameters

Parameter	Value	Units	Location
Ambient Temperature	297	K	Table 1
H_2 Tank Pressure	13.45	MPa	Table 1
H_2 Tank Volume	0.00363	m^3	Table 1
Leak Diameter	0.00356	m	Table 1
Discharge Coefficient-Orifice	0.75	N/A	Table 1

Table A-2 Schefer et al. [20] Figure 4 Input Parameters

Parameter	Value	Units	Location
Tank Temperature	290	K	Figure 4
Tank Pressure	43.1	MPa	Figure 4
Volume H_2	1234	L	Section 3.1
Leak Diameter	5.08	mm	Section 3.1

Table A-3 Proust et al. [21] Figure 4 Input Parameters

Parameter	Value	Units	Location
Orifice Diameter	2	mm	Figure 4
Tank Pressure	90	MPa	Section 2
Tank Volume	25	L	Proust Section 2.0 Page 2
Initial Tank Temperature	315.15	K	Table 1

Table A-4 Schefer et al. [22] Figure 3b Input Parameters

Parameter	Value	Units	Location
Tank Temperature	270	K	Section 2.1, range between 258–284
Tank Pressure	15.5	MPa	Section 2.1
Leak Diameter	3.175	mm	Figure 3
Volume H_2	0.98	m^3	Figure 3 via Riemann sum

A.2. Unignited Jets/Gas Plumes Input Parameters

Table A-5 Molkov [23] Table 5-3 Input Parameters

Original Authors	Temperature (K)	Pressure (bar)	Diameter (mm)	Location
Chaineaux et al.	207	3.6	6	Table 5-3
Chaineaux et al.	174	1.8	12	Table 5-3
Ruffin et al.	288	3.24	25	Table 5-3
Ruffin et al.	288	1.8	50	Table 5-3
Ruffin et al.	288	0.75	75	Table 5-3
Ruffin et al.	288	0.26	100	Table 5-3
Kuznetsov	287	16.1	0.25	Table 5-3
Kuznetsov	287	10.6	0.75	Table 5-3
Kuznetsov	287	9.7	1	Table 5-3
Kuznetsov	287	5.3	1	Table 5-3
Shirvill et al.	287	10	3	Table 5-3
Shirvill et al.	287	13.5	3	Table 5-3
Shirvill et al.	287	2.5	12	Table 5-3
Okabayashi et al.	288	20	2	Table 5-3
Okabayashi et al.	288	40	0.25	Table 5-3
Okabayashi et al.	288	40	0.5	Table 5-3
Okabayashi et al.	288	40	1	Table 5-3
Okabayashi et al.	288	40	2	Table 5-3
Veser et al.	298	5.43	1	Table 5-3
Veser et al.	80	2.99	1	Table 5-3
Veser et al.	298	1.01	2	Table 5-3
Veser et al.	80	1.81	2	Table 5-3

Table A-6 Houf and Schefer [6] Figure 5 Input Parameters

Parameter	Value	Units	Location
Density Exit	0.0838	kg/m^3	Table 1
Ambient Temperature	294	K	Section 2.1 [40]
Ambient Pressure	100	kPa	Section 5
Orifice Diameter	1.905	mm	Figure 5
Mass Flow Rate (Fr=268)	133.91	m/s	Table 1

Table A-7 Houf and Schefer [6] Figure 8 Input Parameters

Parameter	Value	Units	Location
Density Exit	0.0838	kg/m^3	Table 1
Ambient Temperature	273	K	Section 5
Ambient Pressure	100	kPa	Section 5
Orifice Diameter	1.905	mm	Figure 5
Mass Flow Rate (Fr=268)	133.91	m/s	Table 1

Table A-8 Houf and Schefer [6] Figure 9 Input Parameters

Parameter	Value	Units	Location
Density Exit	0.0838	kg/m^3	Table 1
Ambient Temperature	273	K	Section 5
Ambient Pressure	100	kPa	Section 5
Orifice Diameter	1.905	mm	Figure 5
Mass Flow Rate (Fr=268)	133.91	m/s	Table 1
Volumetric Flow Rate (Fr=268)	22.9	slm	Table 1
Mass Flow Rate (Fr=152)	76.02	m/s	Table 1
Volumetric Flow Rate (Fr=152)	13.08	slm	Table 1
Mass Flow Rate (Fr=99)	49.689	m/s	Table 1
Volumetric Flow Rate (Fr=99)	3.5	slm	Table 1

Table A-9 Ruggles and Ekoto [24] Figure 7 Input Parameters

Parameter	Value	Units	Location
Orifice Diameter	1.5	mm	Section 2.1
H_2 Pressure	983.2	kPa	Section 2.1, 10:1 pressure ratio (stagnation to ambient pressure) dynamic feedback was used to maintain a steady pressure ratio
Tank Temperature	295.4	K	Section 2.1
Discharge Coefficient	0.979	N/A	Section 2.1
Ambient Pressure	98.37	kPa	Section 2.1
Ambient Temperature	296	K	Section 2.1

Table A-10 Han et al. [25] Figure 3 Input Parameters

Sub-Figure	Parameter	Value	Units	Location
All	Orifice Diameter 1	0.5	mm	Figure 3
All	Orifice Diameter 2	0.7	mm	Figure 3
All	Orifice Diameter 3	1	mm	Figure 3
All	Initial H_2 Temperature	293	K	Section 3.2
A	Initial Pressure	100	bar	Figure 3a
B	Initial Pressure	200	bar	Figure 3b
C	Initial Pressure	300	bar	Figure 3c
D	Initial Pressure	400	bar	Figure 3d

Table A-11 Han et al. [25] Figure 6 Input Parameters

Sub-Figure	Parameter	Value	Units	Location
All	Initial Pressure 1	100	bar	Figure 6
All	Initial Pressure 2	200	bar	Figure 6
All	Initial Pressure 3	300	bar	Figure 6
All	Initial Pressure 4	400	bar	Figure 6
All	Initial H_2 Temperature	293	K	Section 3.2
A	Orifice Diameter	0.5	mm	Figure 6a
B	Orifice Diameter	0.7	mm	Figure 6b
C	Orifice Diameter	1	mm	Figure 6c

Table A-12 Han et al. [25] Figure 7 Input Parameters

Sub-Figure	Parameter	Value	Units	Location
All	Initial Pressure	300	bar	Figure 7
All	Initial H_2 Temperature	293	K	Section 3.2
A	Orifice Diameter	0.5	mm	Figure 7a
B	Orifice Diameter	0.7	mm	Figure 7b
C	Orifice Diameter	1	mm	Figure 7c

Table A-13 Han et al. [25] Figure 8 Input Parameters

Sub-Figure	Parameter	Value	Units	Location
All	Orifice Diameter	0.7	mm	Figure 8
All	Initial H_2 Temperature	293	K	Section 3.2
A	Initial Pressure	100	bar	Figure 8a
B	Initial Pressure	200	bar	Figure 8b
C	Initial Pressure	300	bar	Figure 8c
D	Initial Pressure	400	bar	Figure 8d

A.3. Ignited Jet Fires Input Parameters

Table A-14 Ekoto et al. [10] Table 2 Input Parameters

Parameter	Value	Units	Location
Flame 1			
Orifice Diameter	20.9	mm	Table 1
Mass Flow Rate	1	kg/s	Table 1
Initial Pressure	59.8	bar_g	Table 1
Initial Temperature	308.7	K	Table 1
Relative Humidity	94.3	%	Table 1
Ambient Temperature	280	bar	Table 1
Ambient Pressure	1.022	K	Table 1
Wind Speed	2.84	m/s	Table 1
Wind Angle	68.5	degrees	Table 1
Visible Flame Length	17.1	m	Table 1
Flame 2			
Orifice Diameter	52.5	mm	Table 1
Mass Flow Rate	7.4	kg/s	Table 1
Initial Pressure	62.1	bar_g	Table 1
Initial Temperature	287.8	K	Table 1
Relative Humidity	94.5	%	Table 1
Ambient Temperature	280	bar	Table 1
Ambient Pressure	1.011	K	Table 1
Wind Speed	0.83	m/s	Table 1
Wind Angle	34	degrees	Table 1
Visible Flame Length	45.9	m	Table 1

Table A-15 Schefer et al. [22] Figure 8 Input Parameters

Parameter	Value	Units	Location
Orifice Diameter	7.94	mm	Schefer and Houf [9]
Tank Temperature	270	K	Section 2.1, range between 258–284
5 s			
Exit Velocity	1233	m/s	Table 1
Volumetric Flow Rate	41026	slm	Table 1
Mass Flow Rate	57.3	g/s	Table 1
20 s			
Exit Velocity	1231	m/s	Table 1
Volumetric Flow Rate	16589	slm	Table 1
Mass Flow Rate	23.17	g/s	Table 1
40 s			
Exit Velocity	1078	m/s	Table 1
Volumetric Flow Rate	4954	slm	Table 1
Mass Flow Rate	6.92	g/s	Table 1
60 s			
Exit Velocity	644	m/s	Table 1
Volumetric Flow Rate	1482	slm	Table 1
Mass Flow Rate	2.07	g/s	Table 1
70 s			
Exit Velocity	446	m/s	Table 1
Volumetric Flow Rate	810	slm	Table 1
Mass Flow Rate	1.13	g/s	Table 1

Table A-16 Houf and Schefer [9] Figure 5 Input Parameters

Parameter	Value	Units	Location	Note
Initial Tank Pressure	2250	psi	Section 3.1	Range of 2000–2500 psi for tank pressure took the midpoint of 2250, blowdown over time
Orifice Diameter	7.94	mm	See note	Schefer and Houf [9]
Tank Temperature	294	K	Section 4	Temperature assumed in paper
Ambient Temperature	294	K	Section 4	Temperature assumed in paper

Table A-17 Houf and Schefer [9] Figure 6 Input Parameters

Parameter	Value	Units	Location	Note
Orifice Diameter	7.94	mm	See Note	Schefer and Houf [9]
Initial Tank Pressure	2250	psi	Section 3.1	Range of 2000–2500 psi for tank pressure, took the midpoint of 2250
Tank Temperature	294	K	Section 4	Temperature assumed in paper
Ambient Temperature	294	K	Section 4	Temperature assumed in paper
Pressure at 5 s	N/A	N/A	N/A	Use exit jet information
Exit Velocity	1233	m/s	Table 1	Schefer and Houf [9]
Volumetric Flow Rate	41026	slm	Table 1	Schefer and Houf [9]
Mass Flow Rate	57.3	g/s	Table 1	Schefer and Houf [9]

Table A-18 Imamura et al. [32] Table 2 Input Parameters

Parameter	Value	Units	Location
Data Set 1			
Orifice Diameter	1	mm	Figure 3
Spouting Pressure 1	1.09	MPa	Figure 3
Spouting Pressure 2	2.17	MPa	Figure 3
Spouting Pressure 3	3.26	MPa	Figure 3
Data Set 2			
Orifice Diameter	2	mm	Figure 3
Spouting Pressure 1	0.47	MPa	Figure 3
Spouting Pressure 2	0.93	MPa	Figure 3
Spouting Pressure 3	1.40	MPa	Figure 3
Spouting Pressure 4	1.87	MPa	Figure 3
Spouting Pressure 5	2.34	MPa	Figure 3
Spouting Pressure 6	2.80	MPa	Figure 3
Data Set 3			
Orifice Diameter	3	mm	Figure 3
Spouting Pressure 1	0.36	MPa	Figure 3
Spouting Pressure 2	0.73	MPa	Figure 3
Spouting Pressure 3	1.09	MPa	Figure 3
Spouting Pressure 4	1.46	MPa	Figure 3
Spouting Pressure 5	1.82	MPa	Figure 3
Spouting Pressure 6	2.19	MPa	Figure 3
Data Set 4			
Orifice Dia.	4	mm	Figure 3
Spouting Pressure 1	0.23	MPa	Figure 3
Spouting Pressure 2	0.47	MPa	Figure 3
Spouting Pressure 3	0.70	MPa	Figure 3
Spouting Pressure 4	0.94	MPa	Figure 3
Spouting Pressure 5	1.17	MPa	Figure 3
Spouting Pressure 6	1.41	MPa	Figure 3

Table A-19 Imamura et al. [32] Table 2 Input Parameters

Parameter	Value	Units	Location
Orifice Diameter	1.0, 2.0, 3.0, and 4.0	mm	Table 2
Spouting Pressure	0.36–3.26	MPa	Table 2

Table A-20 Mogi et al. [33] Figure 9 Input Parameters

Parameter	Value	Units	Location
Orifice Diameter 1	0.002	mm	Figure 9
Orifice Diameter 2	0.0008	mm	Figure 9
Orifice Diameter 3	0.0004	mm	Figure 9
Pressure	35	MPa	Section 3.3
Tank Volume	0.184	m^3	Section 2

Table A-21 Proust et al. [21] Figure 8 Input Parameters

Parameter	Value	Units	Location
Tank Pressure	90	MPa	Section 2
Tank Volume	25	L	Proust Section 2.0 Page 2
Initial Tank Temperature	315.15	K	Table 1
Orifice Diameter 1	3	mm	Figure 8
Orifice Diameter 2	2	mm	Figure 8
Orifice Diameter 3	1	mm	Figure 8

Table A-22 Proust et al. [21] Figure 10 Input Parameters

Parameter	Value	Units	Location
Orifice Diameter	2	mm	Figure 10
Tank Pressure	90	MPa	Figure 10
Tank Volume	25	L	Proust Section 2.0 Page 2
Initial Tank Temperature	315.15	K	Table 1
Flux number 1	(1, 1.41)	m	Figure 3
Flux number 2	(1.5,2.12)	m	Figure 3
Flux number 3	(2, 2.83)	m	Figure 3
Flux number 4	(3, 4.24)	m	Figure 3
Flux number 5	(4, 5.65)	m	Figure 3

A.4. Indoor Accumulation and Overpressure Input Parameters

Table A-23 Ekoto et al. [19] Figure 9 Input Parameters

Parameter	Value	Units	Location
Ambient Pressure	101325	Pa	Assumed
Ambient Temperature	297	K	Assumed
H_2 Tank Pressure	13450000	Pa	Table 1
H_2 Tank Temperature	297	K	Table 1
H_2 Tank Volume	0.00363	m^3	Table 1
Leak Diameter	0.00356	m	Table 1
Discharge Coefficient-Orifice	0.75	N/A	Table 1
Discharge Coefficient-Release	1	N/A	Assumed
Release Area	0.0171	m^2	Figure 2, Section 2.2
Release Height	0.2495	m	Figure 2, Section 2.2
Enclosure Height	2.72	m	Figure 2, Section 2.2
Floor/Ceiling Area	16.722	m^2	Figure 2, Section 2.2
Distance from Release to Wall	2.1255	m	Figure 2, Section 2.2
Angle of Release (0=Horizontal)	0	Radians	Picture
No Ventilation			
Vent 1 (Ceiling Vent) Cross-Sectional Area	0.00865	m^2	Table 3
Vent 1 (Ceiling Vent) Height from Floor	2.42	m	Picture
Vent 2 (Floor Vent) Cross-Sectional Area	0	m^2	Picture
Vent 2 (Floor Vent) Height from Floor	0	m	Picture
Vent Volumetric Flow Rate	0	m^3/min	Picture
With Ventilation			
Vent 1 (Ceiling Vent) Cross-Sectional Area	0.1	m^2	Table 3
Vent 1 (Ceiling Vent) Height from Floor	2.42	m	Picture
Vent 2 (Floor Vent) Cross-Sectional Area	0	m^2	Picture
Vent 2 (Floor Vent) Height from Floor	0	m	Picture
Vent Volumetric Flow Rate	6.5	m^3/min	Table 3

Table A-24 Ekoto et al. [19] Figure 9 Sensor Locations

Sensor	Location Coordinates	Units	Location
S04	(1.97, 1.25, 2.68)	(m, m, m)	Table and Figure 2: Ceiling location distances from vent
S08	(4.16, 1.27, 2.67)	(m, m, m)	Table and Figure 2: Ceiling location, distances from vent
S11	(4.15, 2.83, 2.68)	(m, m, m)	Table and Figure 2: Ceiling location, distances from vent
S04	(0.327, 0, 2.68)	(m, m, m)	Table and Figure 2: Ceiling location, in relation to release point
S08	(-1.86, 0, 2.67)	(m, m, m)	Table and Figure 2: Ceiling location, in relation to release point
S11	(-1.85, 1.58, 2.68)	(m, m, m)	Table and Figure 2: Ceiling location, in relation to release point

Table A-25 Ekoto et al. [19] Figure 14 Input Parameters

Parameter	Value	Units	Location
Ambient Pressure	101325	Pa	Assumed
Ambient Temperature	297	K	Assumed
H_2 Tank Pressure	13450000	Pa	Table 1
H_2 Tank Temperature	297	K	Table 1
H_2 Tank Volume	0.00363	m^3	Table 1
Leak Diameter	0.00356	m	Table 1
Discharge Coefficient-Orifice	0.75	N/A	Table 1
Discharge Coefficient-Release	1	N/A	Assumed
Release Area	0.0171	m^2	Figure 2, Section 2.2
Release Height	0.2495	m	Figure 2, Section 2.2
Enclosure Height	2.72	m	Figure 2, Section 2.2
Floor/Ceiling Area	16.722	m^2	Figure 2, Section 2.2
Distance from Release to Wall	2.1255	m	Figure 2, Section 2.2
Angle of Release (0=Horizontal)	0	Radians	Picture
Test 12			
Vent 1 (Ceiling Vent) Cross-Sectional Area	0.00368	m^2	Figure 14
Vent 1 (Ceiling Vent) Height from Floor	2.42	m	Figure 14
Vent 2 (Floor Vent) Cross-Sectional Area	0	m^2	Figure 14
Vent 2 (Floor Vent) Height from Floor	0	m	Figure 14
Vent Volumetric Flow Rate	0	m^3/min	Figure 14
Ignition Location	Near Forklift	N/A	Table 3
Ignition Delay	3	s	Table 3
Test 11			
Vent 1 (Ceiling Vent) Cross-Sectional Area	0.09716	m^2	Figure 14
Vent 1 (Ceiling Vent) Height from Floor	2.42	m	Figure 14
Vent 2 (Floor Vent) Cross-Sectional Area	0	m^2	Figure 14
Vent 2 (Floor Vent) Height from Floor	0	m	Figure 14
Vent Volumetric Flow Rate	0	m^3/min	Figure 14
Ignition Location	Near Forklift	N/A	Table 3
Ignition Delay	3	s	Table 3
Test 10			
Vent 1 (Ceiling Vent) Cross-Sectional Area	0.09716	m^2	Figure 14
Vent 1 (Ceiling Vent) Height from Floor	2.42	m	Figure 14
Vent 2 (Floor Vent) Cross-Sectional Area	0	m^2	Figure 14
Vent 2 (Floor Vent) Height from Floor	0	m	Figure 14
Vent Volumetric Flow Rate	0	m^3/min	Figure 14
Vent Volumetric Flow Rate	6.3	m^3/min	Figure 14
Ignition Location	Near Forklift	s	Table 3
Ignition Delay	3	m^2	Table 3

Table A-26 Giannissi et al. [34] Figure 7 Input Parameters

Parameter	Value	Units	Location
Ambient Pressure	101325	Pa	Assumed
Ambient Temperature	287	K	Assumed
H_2 Tank Pressure	1700000	Pa	Experimental Description
H_2 Tank Temperature	285	K	Experimental Description
H_2 Tank Volume	N/A	m^3	Mass Flow Controller used
Leak Diameter	0.00055	m	Experimental Description
Release Area	N/A	m^2	Hooker 2013 conference paper, H_2 released from leak diameter directly
Release Height	0.5	m	Experimental Description
Enclosure Height	2.5	m	Figure 1
Floor/Ceiling Area	12.5	m^2	Figure 1
Distance from Release to Wall	2.5	m	Figure 1 and abstract
Vent 1 (Ceiling Vent) Cross-Sectional Area	0.2241	m^2	Table 1
Vent 1 (Ceiling Vent) Height from Floor	2.13	m	Distance to the bottom of the vent
Vent 2 (Floor Vent) Cross-Sectional Area	N/A	m^2	Picture
Vent 2 (Floor Vent) Height from Floor	N/A	m	Picture
Angle of Release (0=Horizontal)	1.5708	Radians	Straight up, Figure 1
Vent Height	0.27	m	Figure 1
Vent Width	0.83	m	Figure 1
Vent Height from Floor (bottom)	2.13	m	Figure 1
Vent Height from Floor (middle)	2.265	m	Figure 1
Vent Height from Floor (top)	2.4	m	Figure 1

Table A-27 Merilo et al. [35] Figure 2 Overall Input Parameters

Parameter	Value	Units	Location
Ambient Pressure	101325	Pa	Assumed
Ambient Temperature	285	K	Assumed
H_2 Tank Pressure	N/A	Pa	Mass Flow Controller used
H_2 Tank Temperature	285	K	Assumed
H_2 Tank Volume	N/A	m^3	Mass Flow Controller used
Leak Diameter	0.00775	m	Section 2, page 3
Release Area	0	m^2	From figure 4, H_2 released from leak diameter directly
Enclosure Height	2.72	m	Section 2, page 2
Floor/Ceiling Area	22.204	m^2	Section 2, page 2
Distance from Release to Wall	0	m	depends on test, see below
Vent 1 (Ceiling Vent) Cross-Sectional Area	0.11	m^2	Section 2
Vent 1 (Ceiling Vent) Height from Floor	2.42	m	Section 2, center of vent
Vent 2 (Floor Vent) Cross-Sectional Area	0.11	m^2	Section 2
Vent 2 (Floor Vent) Height from Floor	0.17	m	Section 2, center of vent 0.08 meters to bottom of vent
Angle of Release (0=Horizontal)	1.5708	Radians	Vertical release, section 2 page 3 and figure 4
Ignition Delay	0	s	depends on test, see below

Table A-28 Merilo et al. [35] Figure 2 Sub-Figure Specific Input Parameters

Parameter	Value	Units	Location
Test 1 - Left			
Release Rate	9.22	kg/h	Table 2
Mass Released	3.07	kg	Table 2
Calculated Exit Velocity	688	m/s	Table 2
Release Duration	20	min	Table 2
Release Height	0.25	m	Table 2
Distance to Wall	4.85	m	Section 2
Vent Flow Rate	0	m^3/s	Table 2
Test 2 - Middle			
Release Rate	9.04	kg/h	Table 2
Mass Released	3.01	kg	Table 2
Calculated Exit Velocity	653	m/s	Table 2
Release Duration	20	min	Table 2
Release Height	1	m	Table 2
Distance to Wall	4.85	m	Section 2
Vent Flow Rate	0	m^3/s	Table 2
Test 3 - Right			
Release Rate	0.88	kg/h	Table 2
Mass Released	0.44	kg	Table 2
Calculated Exit Velocity	63	m/s	Table 2
Release Duration	30	min	Table 2
Release Height	1	m	Table 2
Distance to Wall	4.85	m	Section 2
Vent Flow Rate	0	m^3/s	Table 2

Table A-29 Merilo et al. [35] Figure 6a Input Parameters

Parameter	Value	Units	Location
Ambient Pressure	101325	Pa	Assumed
Ambient Temperature	285	K	Assumed
H_2 Tank Pressure	N/A	Pa	Mass Flow Controller used
H_2 Tank Temperature	285	K	Assumed
H_2 Tank Volume	N/A	m^3	Mass Flow Controller used
Leak Diameter	0.00775	m	Section 2, page 3
Release Area	0	m^2	From figure 4, H_2 released from leak diameter directly
Enclosure Height	2.72	m	Section 2, page 2
Floor/Ceiling Area	22.204	m^2	Section 2, page 2
Distance from Release to Wall	0	m	depends on test, see below
Vent 1 (Ceiling Vent) Cross-Sectional Area	0.11	m^2	Section 2
Vent 1 (Ceiling Vent) Height from Floor	2.42	m	Section 2, center of vent
Vent 2 (Floor Vent) Cross-Sectional Area	0.11	m^2	Section 2
Vent 2 (Floor Vent) Height from Floor	0.17	m	Section 2, center of vent 0.08 meters to bottom of vent
Angle of Release (0=Horizontal)	1.5708	Radians	Straight up, section 2 page 3 and figure 4
Ignition Delay	0	s	depends on test, see below
Release Rate	6.7	kg/h	Table 2
Mass Released	4.47	kg	Table 2
Calculated Exit Velocity	502	m/s	Table 2
Release Duration	40	min	Table 2
Release Height	0.25	m	Table 2
Distance to Wall	3.04	m	Section 2
Vent Flow Rate	0.1	m^3/s	Table 2

Table A-30 Bernard-Michel and Houssin-Agbomson [36] Figure 7 Input Parameters

Parameter	Value	Units	Location
Ambient Pressure	101325	Pa	Assumed
Ambient Temperature	286	K	Table 2
H_2 Tank Pressure	N/A	Pa	Mass Flow Controller
H_2 Tank Temperature	286	K	Mass Flow Controller
H_2 Tank Volume	N/A	m^3	Not Listed, 1E6 used in code
Leak Diameter 1	0.0272	m	Section 3.1
Leak Diameter 2	0.004	m	Section 3.1
Release Area	N/A	m^2	H_2 released from leak diameter directly
Release Height	0.27	m	Section 3.1
Enclosure Height	2.1	m	Section 3.1
Floor/Ceiling Area	0.9216	m^2	Section 3.1
Distance from Release to Wall	0.48	m	Section 3.1
Vent 1 (Ceiling Vent) Cross-Sectional Area	0.1862	m^2	Section 3.1
Vent 1 (Ceiling Vent) Height from Floor	1.7	m	Rough estimation
Vent 2 (Floor Vent) Cross-Sectional Area	0.1862	m^2	Section 3.1
Vent 2 (Floor Vent) Height from Floor	0.02	m	Figure 2
Vent Volumetric Flow Rate	0	m^3/s	Natural Vent
Angle of Release (0=Horizontal)	1.5708	Radians	Figure 1

Table A-31 Bernard-Michel and Houssin-Agbomson [36] Figure 9 Input Parameters

Parameter	Value	Units	Location
Parameter	Value	Units	Location
Ambient Pressure	101325	Pa	Assumed
Ambient Temperature	286	K	Table 2
H_2 Tank Pressure	N/A	Pa	Mass Flow Controller
H_2 Tank Temperature	286	K	Mass Flow Controller
H_2 Tank Volume	N/A	m^3	Not Listed, 1E6 used in code
Leak Diameter 1	0.0272	m	Section 3.1
Leak Diameter 2	0.004	m	Section 3.1
Release Area	N/A	m^2	H_2 released from leak diameter directly
Release Height	0.08	m	Section 3.1
Enclosure Height	1	m	Section 3.1
Floor/Ceiling Area	0.990025	m^2	Section 3.1
Distance from Release to Wall	0.4975	m	Section 3.1
Vent 1 (Ceiling Vent) Cross-Sectional Area	0.1728	m^2	Section 3.1
Vent 1 (Ceiling Vent) Height from Floor	0.75	m	Rough estimation
Vent 2 (Floor Vent) Cross-Sectional Area	0.1728	m^2	Section 3.1
Vent 2 (Floor Vent) Height from Floor	0.02	m	Figure 2
Vent Volumetric Flow Rate	0	m^3/s	Natural Vent
Angle of Release (0=Horizontal)	1.5708	Radians	Figure 1

A.5. Cryogenic Hydrogen Input Parameters

A.5.1. Blowdown

Table A-32 Friedrich et al. [39] Dataset Input Parameters

Graph	Pressure (bar)	Temperature (K)	Diameter (mm)	Location
A	5	80	1	Directly from dataset, see Tables 2 and 3
B	20	80	1	Directly from dataset, see Tables 2 and 3
C	100	80	1	Directly from dataset, see Tables 2 and 3
D	200	80	0.5	Directly from dataset, see Tables 2 and 3
E	200	80	1	Directly from dataset, see Tables 2 and 3
F	200	80	2	Directly from dataset, see Tables 2 and 3
G	200	80	4	Directly from dataset, see Tables 2 and 3
H	200	300	1	Directly from dataset, see Tables 2 and 3

A.5.2. Unignited Jet Plumes

Table A-33 Xiao et al. [37] Figure 3 Input Parameters

Case	Pressure (bar)	Temperature (K)	Diameter (mm)	Location
1	17	298	2	Table 1
2	68.5	298	1	Table 1
3	8.25	80	2	Table 1
4	32	80	1	Table 1

Table A-34 Friedrich et al. [38] Figure 5 Input Parameters

Experiment number	Pressure (bar)	Temperature (K)	Diameter (mm)	Location
3000	19	37	1	Table 1
3002	15	38	1	Table 1
3004	29	36	1	Table 1
3005	18	36	1	Table 1
5001	29.85	43.59	0.5	Table 1
5002	29.85	43.59	0.5	Table 1

Note that the below graph location numbers are from Figures 3-26 and 3-27 in the main body of the report in conventional matrix notation.

Table A-35 Hecht and Panda [13] Figure 10 Input Parameters

Graph Location Number	Pressure (bar)	Temperature (K)	Diameter (mm)	Location
11	2	58	1	Table 1
12	3	56	1	Table 1
13	4	53	1	Table 1
21	5	50	1	Table 1
22	2	61	1.25	Table 1
23	2.5	51	1.25	Table 1
31	3	51	1.25	Table 1
32	3.5	55	1.25	Table 1
33	4	54	1.25	Table 1
41	4	45	1.25	New data
42	2	58	1	New data
43	2	82	1	New data
51	2.5	55	1	New data
52	3	40	1	New data
53	3	63	1	New data

Refer to Table A-32 for the Friedrich et al. [39] input parameters, they are the same for both blowdown and jet plumes.

A.5.3. Ignited Jet Fires

Table A-36 Panda and Hecht [12] Table 3 Input Parameters

Test ID	Pressure (bar-gauge)	Temperature (K)	Diameter (mm)	Location
1	2	163	0.75	Table 3
2	5	179	0.75	Table 3
3	6	205	0.75	Table 3
4	2	215	0.75	Table 3
5	2	46	1.0	Table 3
6	2	55	1.0	Table 3
7	2	62	1.0	Table 3
8	4	78	1.0	Table 3
9	5	81	1.0	Table 3
10	3	113	1.0	Table 3
11	4	124	1.0	Table 3
12	2	127	1.0	Table 3
13	3	163	1.0	Table 3
14	3	175	1.0	Table 3
15	6	295	1.0	Table 3
16	2	46	1.25	Table 3
17	2	53	1.25	Table 3
18	2	64	1.25	Table 3
19	3	70	1.25	Table 3
20	5	91	1.25	Table 3
21	2	144	1.25	Table 3
22	5	155	1.25	Table 3
23	2	185	1.25	Table 3
24	6	200	1.25	Table 3
25	5	272	1.25	Table 3

DISTRIBUTION

Email—External (encrypt for OUO)

Name	Company Email Address	Company Name
Laura Hill	laura.hill@ee.doe.gov	DOE HFTO

Email—Internal (encrypt for OUO)

Name	Org.	Sandia Email Address
Ethan Hecht	08367	ehecht@sandia.gov
Joseph Ronevich	08367	jaronev@sandia.gov
Chris San Marchi	08367	cwsanma@sandia.gov
Brian Ehrhart	08854	bdehrha@sandia.gov
Chris LaFleur	08854	aclafle@sandia.gov
Jamal Mohmand	08854	jamohma@sandia.gov
Scott Sanborn	08854	sesanbo@sandia.gov
Technical Library	1911	sanddocs@sandia.gov

Sandia National Laboratories

Sandia National Laboratories is a multimission laboratory managed and operated by National Technology & Engineering Solutions of Sandia LLC, a wholly owned subsidiary of Honeywell International Inc., for the U.S. Department of Energy's National Nuclear Security Administration under contract DE-NA0003525.